Iron isotopic fractionation driven by low-temperature biogeochemical processes

Nang-Htay Yin, Pascale Louvat, Aubin Thibault-De-Chanvalon, Mathieu Sebilo, David Amouroux

Iron isotopic fractionation driven by low-temperature biogeochemical processes

Nang-Htay YIN, Pascale Louvat, Aubin Thibault-DE-Chanvalon, Mathieu Sebilo, David Amouroux

PII: S0045-6535(23)00068-1

DOI: https://doi.org/10.1016/j.chemosphere.2023.137802

Reference: CHEM 137802

To appear in: *ECSN*

Received Date: 22 September 2022

Revised Date: 6 January 2023

Accepted Date: 8 January 2023

Please cite this article as: YIN, N.-H., Louvat, P., Thibault-DE-Chanvalon, A., Sebilo, M., Amouroux, D., Iron isotopic fractionation driven by low-temperature biogeochemical processes, *Chemosphere* (2023), doi: https://doi.org/10.1016/j.chemosphere.2023.137802.

Author Contribution Statement

Nang-Htay YIN (Main author, conceptualization, data curation, formal analysis, writing of original draft, editing according to co-authors' input, and final submission)

Pascale LOUVAT (Stable isotope and mass spectrometry expert, supervision, validation, review and editing)

Aubin THIBAULT-DE-CHANVALON (Internal review)

Mathieu SEBILO (The first author has been requested to add this additional co-author by last co-author)

David AMOUROUX (Project leader, Funding acquisition, Revision)

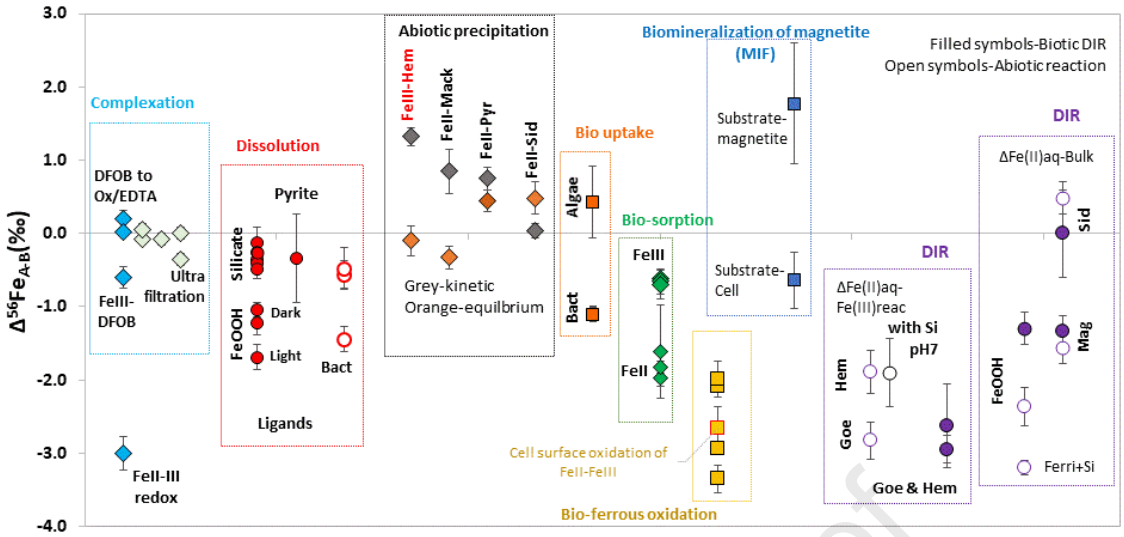

Figure 1. Overview of iron isotopes fractionation driven by low-temperature biogeochemical processes such as redox reaction ($\Delta^{56}Fe_{II\text{-}III}$), ligand-complexation ($\Delta^{56}Fe_{III\text{-}ligands}$), alteration/dissolution ($\Delta^{56}Fe_{solution\text{-}solid}$), abiotic mineral precipitation ($\Delta^{56}Fe_{II/III\text{-}mineral}$), bio-uptake ($\Delta^{56}Fe_{III\text{-}cell}$), bio-sorption ($\Delta^{56}Fe_{II\text{-}biomass}$ vs $\Delta^{56}Fe_{III\text{-}biomass}$), microbial oxidation ($\Delta^{56}Fe_{II\text{-}III\text{-}FeOOH}$), biomineralization ($\Delta^{56}Fe_{II\ or\ III\text{-}mineral/cell}$) and dissimilatory iron reduction of iron minerals ($\Delta^{56}Fe_{FeIIaq\text{-}FeIIIreact}$ and $\Delta^{56}Fe_{FeIIaq\text{-}BulkMineral}$). (DFOB-desferrioxamine B, FeOOH-oxyhydroxide minerals, Bact-bacteria, Hem-hematite, Fer-ferrihydrite, Goe-goethite, Mag-magnetite, Sid-siderite, Mack-mackinawite, Pyr-pyrite, and DIR- dissimilatory iron reduction). In the "Dissolution" box, light refers to the presence of light favoring photochemical reductive dissolution and dark refers to the absence of light favoring oxidative dissolution. The red outline of one symbol in the "Bio-ferrous oxidation" box corresponds to the calculation of $\Delta^{56}Fe$ between $FeII_{aq}$ and FeIII on cell surface while the rest of calculation focused between FeII-FeIII and precipitated FeIII minerals. In the "DIR" box, the open symbol with black outline corresponds to the abiotic hematite experiment conducted in the presence of Si at pH7 in comparison to the experiments without Si. Error bars represent 2SD experimental error and. Detailed values and corresponding references for each process are given in Table 1, 2 and 3

18

Iron Isotopic Fractionation Driven by Low-Temperature Biogeochemical Processes

Nang-Htay YIN[1], Pascale LOUVAT[1], Aubin THIBAULT-DE-CHANVALON[1], Mathieu SEBILO[1,2], David AMOUROUX[1]

[1]Universite de Pau et des Pays de L'Adour, E2S UPPA, CNRS, IPREM, Institut des Sciences Analytiques et de Physico-chimie pour L'Environnement et Les Matériaux, Pau, France

[2]Sorbonne Université, CNRS, IEES, Paris, France

Corresponding author: nang-htay.yin@univ-pau.fr, nangsao87@gmail.com

Corresponding address: IPREM (Institut des sciences analytiques et de physico-chimie pour l'environnement et les matériaux), Technopole Hélioparc, 2 avenue du Président Pierre Angot, 64053 Pau, France.

Abstract

Iron is geologically important and biochemically crucial for all microorganisms, plants and animals due to its redox exchange, the involvement in electron transport and metabolic processes. Despite the abundance of iron in the earth crust, its bioavailability is very limited in nature due to its occurrence as ferrihydrite, goethite, and hematite (Crichton, 2001) where they are thermodynamically stable with low dissolution kinetics in neutral or alkaline environments. Organisms such as bacteria, fungi, and plants have evolved iron acquisition mechanisms to increase its bioavailability in such environments, thereby, contributing largely to the iron cycle in the environment. Biogeochemical cycling of metals including Fe in natural systems usually results in stable isotope fractionation; the extent of fractionation depends on processes involved. Our review suggests that significant fractionation of iron isotopes occurs in low-temperature environments, where the extent of fractionation is greatly governed by several biogeochemical processes such as redox reaction, alteration, complexation, adsorption, oxidation and reduction, with or without the influence of microorganisms. This paper includes relevant data sets on the theoretical calculations, experimental prediction, as well as laboratory studies on stable iron isotopes fractionation induced by different biogeochemical processes.

Keywords

Iron isotopes, fractionation, biogeochemical processes, microbial uptake, ligands

1. Introduction

Iron is the fourth most abundant element in the Earth's crust and is present in natural aquatic environment at varying quantities depending upon the background geology and type of waterway; marine, rivers or acid-mine (USEPA 1986). Despite its abundance, iron is mostly present as various iron (oxyhydro)oxides such as ferrihydrite, goethite, and hematite. Their solubility is limited and controlled by other environmental parameters, leading to poor bioavailability in nature. Being an essential element for plants, animals and microorganisms, iron is actively involved in many biogeochemical processes.

Iron biogeochemical cycle in nature has an important role over other elemental cycles; notably oxygen, sulfur, mercury, and other transitional elements like zinc, copper, chromium or nickel. For instance, Fe as an essential element for life, bacteria to plants and vertebrates, affect carbon and nitrogen cycles, ocean biological production and organic matter mineralization and production of climate effective biogenic gases. Dissolved FeS and mackinawite mineral affect the degradation of dimethyl-mercury in the ocean, thereby controlling in part biogeochemical cycle of mercury. Likewise, the formation of different Fe (oxyhydro)oxides in oxidative environments is well-known for scavenging transitional metals like Zn, Cu, Ni and Cr via coprecipitation and adsorption, thereby, effecting not only their biogeochemical cycles but also their respective isotopic fractionation. It is important to understand Fe geochemical cycles and its isotopic fractionations as it could help solve the fundamental questions involving other elemental cycles as well.

Understanding the biogeochemical transformation of iron in terrestrial and aquatic ecosystems has been promising, thanks to the developments in Multicollector-Inductively Coupled Plasma Mass Spectrometer (MC-ICPMS) and stable iron isotopes. A large number of studies were conducted over the last ~20 years investigating Fe isotope fractionation in various experimental and field studies, as well as many theoretical calculations. Recent literature

reviews with larger scope involve iron isotope systematics in both terrestrial and extraterrestrial systems (Dauphas et al., 2016; 2017); iron cycling and isotope fractionation in terrestrial ecosystems (Wu et al., 2019); and iron isotopes in modern surficial world and the ancient earth (Johnson et al., 2020). Therefore, this review article will focus on the available theoretical and experimental data on stable iron isotope fractionation during various low-temperature biogeochemical processes in microenvironments or at a cellular level. The aim is to reorganize the existing data set, to identify the limitations of applying iron isotopes in differentiating the abiotic processes from microbial iron recycling, and to point out future research direction.

Our review suggests that significant fractionation of iron isotopes occurs in low-temperature environments, where the extent of fractionation is greatly governed by several biogeochemical processes such as redox reaction, alteration, complexation, adsorption, oxidation and reduction, where overlapping signatures is observed between abiotic and biotic contribution. The influence of microorganisms is isotopic iron fractionation is too weak compared to our understanding/the complexity of iron cycling to use iron isotope as a tracer for biotic influences. Our understanding remains even poorer when it comes to the microbially-driven fractionation at intracellular and extracellular levels, therefore providing a great opportunity for future work.

2. Overview of biogeochemical processes inducing iron isotopes fractionation

Figure 1 represents biogeochemical cycling of iron in nature involving several processes such as redox reactions, ligand-complexation, dissolution (biotic and abiotic), precipitation from FeII or/and FeIII source (abiotic), bioassimilation (bio-uptake, bio-sorption, biomineralization, dissimilatory iron reduction processes). Detailed values and corresponding references for each process are given in Table 1, 2, 3 and 4.

The simple redox reactions between FeII and FeIII could induce $\Delta^{56}Fe_{II\text{-}III}$ of −3.00±0.23‰ as calculated by several experimental studies (Table 2), whereas the complexation of FeIII and desferrioxamine B (DFOB) ligand induce less fractionation, $\Delta^{56}Fe_{III\text{-}DFOB}$ of −0.60±0.15‰

(Table 2). During mineral weathering, the fractionation induced by both abiotic and biotic influence is overlapped for all minerals (silicates/phyllosilicates and oxyhydroxides). Nonetheless, the fractionation is rather distinguished by the isotopic signatures of the original minerals. The observed fractionation induced by ligand or proton promoted dissolution, $\Delta^{56}Fe_{sol\text{-}solid}$ is −0.32±0.13‰ for silicates/phyllosilicates dissolution, whereas $\Delta^{56}Fe_{sol\text{-}solid}$ is −1.22±0.17‰ for oxyhydroxide dissolution. Photochemically driven reductive dissolution resulted in more negative $\Delta^{56}Fe$ values than dark dissolution (in absence of light) as the presence of light activates the photo-reactive functional groups on the oxalic ligands accommodating reductive mechanisms.

Abiotic precipitation of oxidized (hematite) or reduced (siderite, mackinawite and pyrite) minerals showed that the extent of Fe isotope fractionation depends strongly on whether kinetic or equilibrium isotope effects are dominant. Degree of saturation, different precipitation rates, dissolution-reprecipitation, mixing interfaces (between mineral surface and solution vs bulk mineral and solution) and the experimental duration could induce significant kinetic isotopic fractionation or could shift the isotopic equilibrium.

Variation in iron isotope fractionation is observed during uptake by different microorganisms, i.e. $\Delta^{56}Fe_{FeIII\text{-}algae}$ is 0.43±0.49‰ for algae as well as $\Delta^{56}Fe_{FeIII\text{-}bact}$ is −1.10±0.11‰ for bacteria. A similar and large variation is observed during the microbial ferrous oxidation, $\Delta^{56}Fe_{FeII\text{-}FeOOH}$ varies from −1.99±0.24‰ to −3.35±0.19‰ depending on the types of microorganisms involved, different metabolic pathways and different surface functional group on cell, as well as the diversity of end mineral formation. Precipitation could take place either in the periplasm, at the cell surface or extracellularly (exopolysaccharides). On the other hand, the bio-mineralization of magnetite by *Magnetospirillum Magneticum strain AMB-1* resulted in a positive $\delta^{56}Fe$ enrichment of FeII and FeIII substrates[1] with respect to

[1] FeII-lysate or FeIII-lysate substrates

magnetite where $\Delta^{56}Fe_{FeII/III\text{-}magnetite}$ is 1.77±0.82‰ (Amor et al., 2016). It is also noteworthy that MIF is observed on ^{57}Fe during biominerization in parallel to other biogeochemical processes.

Bio-sorption of both FeII and FeIII onto the microbial biomass can be expected in parallel other microbial processes. The extent of fractionation due to bio-sorption is −1.81±0.18‰ for $\Delta^{56}Fe_{FeII\text{-}cell}$ and −0.66±0.04‰ for $\Delta^{56}Fe_{FeIII\text{-}cell}$ during the incubation of planktonic cyanobacteria (*Gloeocapsa sp., Synehococcus sp.,* and *Planthothrix sp.*) in FeII and FeIII substrates. Fractionation is presumably linked to changes of the Fe coordination chemistry between the aqueous phase and cells surface. The surface carboxyl and phosphoryl groups could interact with both FeII and FeIII through covalent binding; therefore, reducing chances of FeIII polymerization and preventing subsequent oxyhydroxides precipitation.

Biotic or abiotic reduction of iron minerals can be expected whenever anoxic and anaerobic conditions are favored in soil, groundwater, and in sediments. Studies have confirmed that the negative $\delta^{56}Fe$ values for aqueous FeII in natural systems reflects dissimilatory iron reduction process (DIR). The second largest range observed was for $\Delta^{56}Fe_{FeIIaq\text{-}FeIIIreact}$, which includes both biotic and abiotic reduction of goethite and hematite (−1.68±0.08‰ to −2.83±0.23‰), while the largest range was observed for microbial ferrous iron oxidation (−1.99±0.24‰ to −3.35±0.19‰)."The extent of fractionation could be shifted further by the presence of dissolved Si, different solution pHs, the natural organic matter or the changes in the mineral structures when these impurities are incorporated. The main mechanism inducing fractionation is due to the isotopic exchange between aqueous FeII and reactive FeIII on the oxide surface for both abiotic and biotic experiments where the role of bacteria was to catalyze the isotopic exchange via electron pumping to the oxide surface. Microbial reduction of ferrihydrite, goethite and hematite could lead to the formation of biogenic oxides and carbonates minerals such as

magnetite and siderite via reprecipitation. The extent of fractionation is primarily controlled by the source signature of the original mineral rather than the biotic or abiotic contribution.

In summary, a wide range of iron isotope fractionation, $\Delta^{56}Fe_{A\text{-}B}$ can be observed across each process (Fig 1 and Table 2, 3, 4); redox reaction between FeII and FeIII (−3.00‰), complexation (−0.60‰ to 0.20‰), dissolution (−1.44‰ to 0.48‰), precipitation (−0.33‰ to 1.30‰), biouptake (−1.1‰ to 0.4‰), biosorption (−2‰ to −0.6‰), bio-oxidation (−3.35‰ to −2.15‰), mineralization (−0.64‰ to 1.77‰), dissimilatory iron reduction (−2.95‰ to −1.68‰). One process can be a subsidiary of another and more than one process may take place simultaneously, where iron isotopes can be useful as a tool to identify which family of geochemical processes is dorminant in place, but not biotic influence from abiotic one.

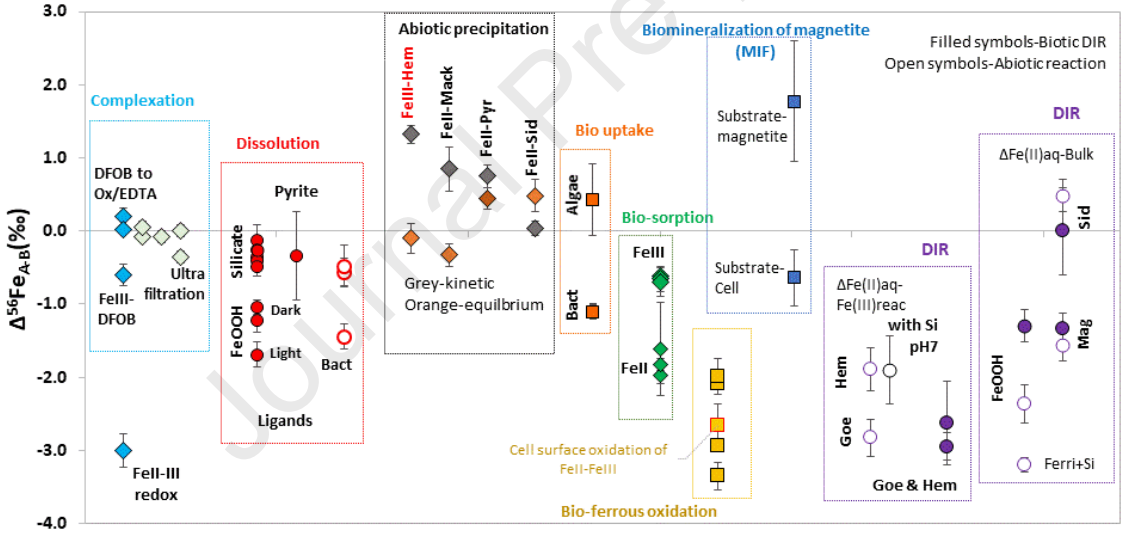

Figure 1. Overview of iron isotopes fractionation driven by low-temperature biogeochemical processes such as redox reaction ($\Delta^{56}Fe_{II\text{-}III}$), ligand-complexation ($\Delta^{56}Fe_{III\text{-}ligands}$), alteration/dissolution ($\Delta^{56}Fe_{solution\text{-}solid}$), abiotic mineral precipitation ($\Delta^{56}Fe_{II/III\text{-}mineral}$), bio-uptake ($\Delta^{56}Fe_{III\text{-}cell}$), bio-sorption ($\Delta^{56}Fe_{II\text{-}biomass}$ vs $\Delta^{56}Fe_{III\text{-}biomass}$), microbial oxidation ($\Delta^{56}Fe_{II\text{-}III\text{-}FeOOH}$), biomineralization ($\Delta^{56}Fe_{II\ or\ III\text{-}mineral/cell}$) and dissimilatory iron reduction of iron minerals ($\Delta^{56}Fe_{FeIIaq\text{-}FeIIIreact}$ and $\Delta^{56}Fe_{FeIIaq\text{-}BulkMineral}$). (DFOB-desferrioxamine B, FeOOH-oxyhydroxide minerals, Bact-bacteria, Hem-hematite, Fer-ferrihydrite, Goe-goethite, Mag-

magnetite, Sid-siderite, Mack-mackinawite, Pyr-pyrite, and DIR- dissimilatory iron reduction). In the "Dissolution" box, light refers to the presence of light favoring photochemical reductive dissolution and dark refers to the absence of light favoring oxidative dissolution. The red outline of one symbol in the "Bio-ferrous oxidation" box corresponds to the calculation of $\Delta^{56}Fe$ between $FeII_{aq}$ and FeIII on cell surface while the rest of calculation focused between FeII-FeIII and precipitated FeIII minerals. In the "DIR" box, the open symbol with black outline corresponds to the abiotic hematite experiment conducted in the presence of Si at pH7 in comparison to the experiments without Si. Error bars represent 2SD experimental error and. Detailed values and corresponding references for each process are given in Table 1, 2 and 3.

3. Detailed overview on Fe isotopes fractionation by different biogeochemical processes

This section represents several experimental studies detailing on each biogeochemical process where abiotic vs biotic contribution, as well as kinetic vs equilibrium Fe isotope fractionation, is further addressed. Experimental fractionation is further compared to the calculated or theoretical fractionation where relevant. It is noteworthy that each geochemical process can be either biotic or abiotic, during which isotope fractionation could be either kinetic-driven, at equilibrium or a convergence of both.

3.1. Redox reactions (abiotic, kinetic and equilibrium)

The iron isotopes are fractionated during redox reactions (oxidation or reduction), either kinetically or at equilibrium. Equilibrium and kinetic iron isotope fractionation between aqueous FeII and FeIII was reported over a range of salinity (0, 11, 110mM Cl^-) and temperatures (0 and 22°C). The average measured equilibrium fractionation; $\Delta^{56}Fe_{II\text{-}III}$ is −3.00±0.23‰ at 22°C whereas it becomes lower, −3.57±0.38‰ at 0°C for all salinity, indicating that fractionation is a function of temperature rather than salinity (Welch et al., 2003). These fractionations are slightly different from the study by Johnson et al. (2002) as they were corrected from experimental errors related to separation and recovery, or partial reaction of FeII

and FeIII during precipitation. Kinetics of iron isotope exchange can be described by a second-order rate equation where the rates are affected by temperature and salinity. The kinetic exchange rates are about an order of magnitude slower at 0°C compared to rapid exchange at 22°C, and 40% slower at the salinity of 11mM Cl^- compared to the rates at 0mM or 100mM Cl^-. The redox exchange between FeII and FeIII is a simple homogenous exchange reaction with a net exchange of one electron between two high-spin Fe atoms. Electron exchange takes place in three steps (Wehrli, B., 1990): the formation of a precursor complex, electron transfer (across a bridging hydroxyl, water, or chlorite ion), and dissociation of the complex, where a series of reactions can be written as follows:

Overall isotopic exchange during redox, $^{56}Fe^{2+} + {}^{54}Fe^{3+} \rightarrow {}^{54}Fe^{2+} + {}^{56}Fe^{3+}$

Precursor formation,

$$[^{56}FeII(H_2O)_6]^{2+} + [^{54}FeIII(H_2O)_5(OH)]^{2+} \rightarrow [(H_2O)_5{}^{54}FeIII(OH)(H_2O).\ {}^{56}FeII(H_2O)_5]^{4+}$$

Electron transfer,

$$[(H_2O)_5{}^{54}FeIII(OH)(H_2O).\ {}^{56}FeII(H_2O)_5]^{4+} \rightarrow [(H_2O)_5{}^{54}FeII(OH)(H_2O).\ {}^{56}FeIII(H_2O)_5]^{4+}$$

Dissociation of complex,

$$[(H_2O)_5{}^{54}FeII(OH)(H_2O).\ {}^{56}FeIII(H_2O)_5]^{4+} \rightarrow [^{56}FeII(H_2O)_6]^{2+} + [^{54}FeIII(H_2O)_5(OH)]^{2+}$$

3.2. Complexation of Fe and organic matter (sub process of every process)

Complexation of Fe to organic molecules could be one of the initial, however, influential processes taking place within each biogeochemical process in nature, where Fe could be either in dissolved, colloidal or particulate form and organic molecules of different sizes (organic matter like humic substances, biological byproducts, bioligands). As an example, the equilibrium Fe isotope fractionation induced by complexation of the reference organic ligand, desferrioxamine B (DFOB) to inorganic FeIII species resulted in a negative $\Delta^{56}Fe_{FeIII\text{-}DFOB}$ of

205 −0.60 ± 0.15‰ as given in Fig 2A (Dideriksen et al., 2008). Fe isotope effects can also be
206 driven by changes in Fe coordination that involve the exchange between different organic
207 ligands. For instance in Fig 2A, the measured equilibrium Fe isotope fractionation between
208 FeIII-DFOB (desferrioxamine B) to FeIII-Ox (Oxalate), and to FeIII-EDTA
209 (ethylenediaminetetraacetic acid) resulted in $\Delta^{56}Fe_{(FeIII\text{-}DFOB)\text{-}(FeIII\text{-}Ox)}$ of 0.20±0.11‰ and
210 $\Delta^{56}Fe_{(FeIII\text{-}DFOB)\text{-}(FeIII\text{-}Ox)}$ of 0.02±0.11‰ (Morgan et al., 2010). In these studies, preferential
211 complexation of heavy Fe isotopes by OM and/or hydroxyl ligands to form stronger chemical
212 bonds is reported (Roe et al., 2003; Dideriksen et al., 2008; Morgan et al., 2010).

213 A similar study on Fe complexation with organic matter at pH 6.5 reported that the relative
214 distribution of Fe and OM depends on different particle size fractions by ultrafiltration (Lotfi-
215 Kalahroodi et al., 2019). Significant Fe isotope fractionation was observed for the smallest
216 particles. As shown in Fig 2A, at circumneutral pH 6.5, 43% of Fe and 57% of OM were in the
217 <0.2 μm fraction and only 0.8% of Fe and 20% of OM were in the <30 kDa fraction. However,
218 the isotope fractionation was only $\Delta^{56}Fe_{TotFe-<0.2\mu m}$ −0.07±0.08‰ for the larger particle size
219 while it was $\Delta^{56}Fe_{TotFe-<30\ kDa}$ −0.35±0.08‰ for the smallest size. As a budget, 42% of Fe and
220 38% of OM were found in the 0.2 μm - 30 kDa fraction with $\Delta^{56}Fe_{TotFe-(0.2\mu m\text{-}30\ kDa)}$ of
221 −0.08±0.08‰ (Lotfi-Kalahroodi et al., 2019)[2]. Fractionation of Fe isotope can be significant
222 depending upon particles' size during Fe complxation with oxyhydroxide/OM to form
223 nanoaggregates at pH 6.5, natural range for aquatic environments and soil pore waters.

224 In complement to experiments, quantum chemical calculations allow to better understand
225 the isotopic effects of Fe speciation and complexation. Reduced partition function ratios
226 between ^{56}Fe and ^{54}Fe, $\beta^{56/54}$ factor[3] (or $10^3Ln\beta^{56/54}$ at 25°C in Fig 2B), depict the magnitude of

[2] The $\Delta^{56}Fe_{A\text{-}B}$ is recalculate based on the $\delta^{56}Fe$ values given in the Table 5 of the publication (Lotfi-Kalahroodi et al., 2019)
[3] Iron reduced partition isotopic function ratio (β factor) is commonly used to calculate magnitude and direction of equilibrium iron isotope fractionation in several theoretical calculation using density functional theory (DFT) modeling and ab-initio calculation. One can say that $10^3Ln\beta^{56/54}$ in calculation studies is similar to $\delta^{56}Fe$ measured in MC-ICPMS and $10^3 \ln \alpha_{A-B}$ will be equivalent to the big delta $\Delta_{A\text{-}B}$, respectively. Please refer to SI for details Nomenclature and Comparability.

the equilibrium isotopic fractionation between different Fe redox species, organic and inorganic ligands, in respect to the bond lengths of the molecules formed. Three different basic fractionations can be expected: (1) redox reaction of Fe within the same phosphate complex ($Fe^{II}HPO_4(H_2O)_5$ & $Fe^{III}HPO_4(H_2O)_5^+$), (2) the exchange between different inorganic ligands but the same Fe redox ($Fe^{III}HPO_4(H_2O)_5^+$ & $Fe^{III}CO_3(H_2O)_4^+$), (3) the exchange between inorganic and organic ligands but the same Fe redox ($Fe^{III}(cit)_2OH_4^-$ & $Fe^{III}Cl_2(H_2O)_4^+$). It is also noteworthy that β factor is inversely proportional to the bond length and that heavy isotopes form shorter bonds than light isotopes. Calculations allows us to predict the order of magnitude Fe isotope fractionation during ligands exchange, and show the expected diversity according to the reactions and bonds involved. Experimental studies to address/verify such theoretical data are however very limited.

3.3. Dissolution (abiotic vs biotic)

Different organic ligands (oxalic acid, acetic acid, citric acid, desferrioxamine mesylate-DFAM) are used to study abiotic dissolution of iron-bearing minerals. Minerals involved in the studies were hornblende (iron silicates), phyllosilicates (biotite/cholorite), pyrites (reduced minerals) and goethite (amorphous mineral). Soil bacteria, *Bacillus mycoides* and *Streptomyces sps* were cultured with the minerals in order to better understand their influence on continental weathering, but also mineral and soil formation (Brantley et al., 2001a,b; 2004, Wiederhold et al., 2006; Jang et al., 2008; Kiczka et al., 2010a; Wolfe et al., 2016).

During the abiotic and biotic dissolution of iron silicates (hornblende and phyllosilicates) given in Figure 2C, the measured offset $\Delta^{56}Fe_{sol\text{-}solid}$ is −0.36±0.25‰ (DFAM), −0.25±0.18‰ (oxalic acid), −0.13±0.21‰ (acetic acid), −0.40±0.21‰ (citric acid), −0.56±0.19‰ (*Bacillus mycoide*s) and −0.48±0.29‰ (*Streptomyces*) respectively. Variation in fractionation among different ligands and different types of soil bacterial strains is insignificant within error, and with overlapping offsets between abiotic and biotic contribution. Fe isotope fractionation is

presumably induced during hydrolysis of surface complexes by ligands where the strength of Fe-ligands complex is greater than that of bonds retaining Fe in the mineral lattice, accentuating the irreversibility of the hydrolysis.

On the other hand, the abiotic and biotic dissolution of goethite (Figure 2C) led to $\Delta^{56}Fe_{sol\text{-}solid}$ of −1.04±0.10‰ (DFAM), −1.2±0.17‰ (oxalic-dark), −1.7±0.17‰ (oxalic-light) and −1.44±0.17‰ (*Bacillus mycoides*). Please note that $\Delta^{56}Fe$ are recalculated from the $\Delta^{57}Fe$ assuming that all the measured data points follow a mass-dependent fractionation. The fractionation observed in oxalic-light experiments indicated photochemical reductive dissolution, promoting electron transfer at the mineral surface that access the crystallographic sites, normally not reactive in ligand controlled (oxalic dark) dissolution (Wiederhold et al., 2006). Similarly, Fe release was enriched in light isotopes in proton promoted dissolution of pyrite by HCl at pH 4-6 with $\Delta^{56}Fe_{sol\text{-}solid}$ of −0.34±0.61‰ (Wolfe et al., 2016). During the proton promoted dissolution of silicates, the exfoliation of the silicate structure is triggered by the release of potassium, which favors the dissolution of an octahedral layer from the edges inwards and leaves the tetrahedral sheets less affected (Kiczka et al., 2010a; Wolfe et al., 2016).

3.4. Mineral precipitation (Abiotic, kinetic and equilibrium)

Only few studies explored the precipitation of iron to minerals via abiotic experiments; hematite at 98°C (Skulan et al., 2002) extrapolated to 25°C (Beard et al., 2010), ferrihydrite at 25°C (Johnson et al., 2002), siderite at 25°C (Wiesli et al., 2004), sulfide between 2 and 40°C (Guilbaud et al., 2010) and goethite at 25°C (Handler et al., 2009). These studies have demonstrated how different rates of mineral precipitation can influence kinetic iron isotope fractionation. High degree of saturation induced high precipitation rates that will induce almost no kinetic fractionation, whereas moderately fast precipitation rates induce significant kinetic fractionation (Johnson et al., 2002; Skulan et al., 2002; Jimenez-Lopez and Romanek, 2004;

276 Wiesli et al., 2004). But if precipitation rates are small enough, each portion of mineral
277 precipitated is in isotopic equilibrium with aqueous Fe, resulting in a global equilibrium.

278 ***Iron oxyhydroxide precipitation:*** Johnson et al., (2002) demonstrated that extremely rapid
279 precipitation within seconds produces no significant iron isotopic fractionation between
280 aqueous FeII in solution and colloidal FeIII oxyhydroxide.

281 ***Hematite precipitation:*** Skulan et al., (2002) demonstrated that moderately rapid
282 precipitation within hours could produce the largest kinetic isotopic fractionation between FeIII
283 and hematite. Beard et al. (2010) extrapolated the precipitation study at 98°C by Skulan et al.
284 (2002) to 25°C. The extrapolated kinetic fractionation, $10^3Ln^{56}\alpha_{FeIIIaq\text{-}hematite\_kinetic}$ is
285 1.32±0.12‰ at 25°C where the extrapolated equilibrium fractionation remains close to zero;
286 $10^3Ln^{56}\alpha_{FeIIIaq\text{-}hematite\_equilibrium}$ is −0.15±0.20‰ at 25°C (Figure 2D). The moderately rapid
287 precipitation rates are more likely to be associated with kinetic isotope fractionation, or largest
288 fractionation observed in the experiment.

289 ***Siderite precipitation:*** Wiesli et al., (2004) also mentioned that super-saturation with high
290 precipitation rate produce almost no fractionation ($\Delta^{56}Fe_{FeIIaq\text{-}siderite\_kinetic}$ of 0.04±0.10‰) in
291 agreement with Johnson et al., (2002). Contrastingly, at moderate precipitation rate Wiesli et
292 al. (2004) mention larger kinetic isotope fractionation, which extend depends on the formed
293 mineral size ($\Delta^{56}Fe_{FeIIaq\text{-}siderite\_10H}$ of 2.06±0.10‰ for >10 µm siderite, vs 0.93±0.10‰ for 0.45-
294 10 µm siderite). The proposed equilibrium fractionation factor between FeII and siderite from
295 regression of all the experimental data is 0.48±0.22‰ ($10^3Ln^{56}\alpha_{FeIIaq\text{-}siderite\_equilirbrium}$).

296 ***Mackinawite precipitation:*** Butler et al. (2005) and Guilbaud et al. (2010) reported the
297 kinetic isotope effects where the isotopic exchange is likely to happen via dissolution-
298 precipitation between the mineral surface and the solution rather than the bulk mineral and the
299 solution. The proposed kinetic isotope fractionation, $\Delta^{56}Fe_{FeIIaq\text{-}mackinawite\_kinetic}$ is 0.85±0.30‰ at

25°C. Guilbaud et al., (2011a) observed that the apparent equilibrium precipitation of mackinawite, $\Delta^{56}Fe_{FeIIaq\text{-}mackinawite\_equilibrium}$ is −0.33±0.16‰ at 25°C (Figure 2D).

Sulfide precipitation: Redox cycling of Fe coupled to pyrite precipitation from sources with either negative $FeII_{aq}$ composition or positive $FeIII_{aq}$ composition display the largest $\delta^{56}Fe$ variation ranging from -4‰ to +4‰ in nature due to its multiple precipitation pathways. The first pathway is via H_2S or polysulfide pathway where formation of aqueous FeS clusters (FeS_{aq})[4] occurs under sulfide-rich conditions (Rickard et al., 2001), the second pathway is via formation of intermediate phase, greigite (Fe_3S_4)[5] and the third pathway is via the ferric-hydroxide-surface (FHS) formation (Peiffer et al., 2015; Wan et al., 2017). As given in Figure 2D, the apparent equilibrium isotopic fractionation between FeII and pyrite, $\Delta^{56}Fe_{FeSx\text{-}Pyrite}$ is 0.54±0.21‰ via H_2S pathway, ranging between 0.41±0.14‰ and 0.59±0.25‰ via polysulfide pathway, and ranging between 0.41±0.23‰ and 0.63±0.04‰ via greigite as intermediate (Mansor and Fantle et al., 2019). Therefore, the average equilibrium isotopic fractionation between FeS_x and pyrite, where FeS_x includes FeS, $FeII_{aq}$ and greigite; $\Delta^{56}Fe_{FeSx\text{-}Pyrite\_equilibrium}$ of 0.51±0.22‰, which is identical within error irrespective of precipitation pathways. The kinetic isotope effect is visible during early stages of precipitation where the proposed fractionation, $\Delta^{56}Fe_{FeSx\text{-}Pyrite\_kinetic}$ is 0.75±0.15‰. Early-stage nucleation vs later-stage crystal growth also contribute to such isotopic variations, where it is difficult to distinguish nucleation effects from kinetic effect.

3.5. Microbial assimilation (uptake, oxidation, mineralization)

Iron is an essential nutrient for all microorganisms, different groups use iron as an electron donor or acceptor to carry out numerous metabolic reactions, thereby contributing to the microbial share of iron redox transformations in nature. Microbial influence could induce iron

[4] FeS clusters are the first form of sulfide precipitates where the long polysulfide chain involves one or more groups of sulfur linked together via covalent bonds

[5] Greigite is has a similar inverse spinel structure where atoms are closely packed cubic array, therefore much more stable.

isotope fractionation in several ways: (1) the direct oxidation of FeII to FeIII, (2) sorption of both FeII and FeIII on to biomass either dead or alive, (3) partial sorption of iron onto microbial precipitated oxyhydroxides, and (4) Fe chelated by bacterial byproducts. Microbial assimilation of iron by microorganisms is the primary process from which several specific processes can be identified and subdivided into bio-uptake, bio-oxidation and bio-mineralization. In addition, bio-sorption, a lateral or indirect process, can take place in parallel to microbial assimilation. Note that the microbial processes in this section 3.5 are taking place in aerobic environments while the following section 3.6 will focus on microbial assimilation in anaerobic environments.

Bio-uptake: Studies have shown that the extent of fractionation due to bacteria is larger compared to that of algae (Figure 2E). The bacterial Fe uptake by the soil bacterium, *Azotobacter vinelandi* gave the fractionation of −1.10±0.06‰ (Wasylenki et al., 2007), different from the algae uptake by *Chlorella pyrenoidosa* (0.08±0.09‰), and *Chlamydomonas reinhardtii* (0.78±0.09‰) respectively (Sun and Wang, 2018). The difference in sign for algae (+) and bacteria (-) of $\Delta^{56}Fe_{III\text{-}cell/algae,}$ is worth further discussion regarding their differences in the uptake mechanisms (phytoplankton vs. bacteria). The algae depicted contrasting Fe isotope compositions in intracellular and extracellular fractions. The intracellular Fe have heavy Fe isotope composition in relative to the initial FeII substrate, whereas the extracellular Fe is isotopically variable hosting a mixture of FeII with light signature and FeIII enriched in heavy isotopes. The oxidation of adsorbed FeII in the extracellular fraction and the selective transport of such isotopically heavy Fe into the cell could account for the fractionation observed in the studies with algae (Sun and Wang, 2018). Bacterium, *A. vinelandii* is known to produce high affinity and stronger Fe chelator, dihydroxybenzoic acid, compared to the Fe-citrate substrate present in the medium. The equilibrium shift between the two pools of Fe is thus responsible for isotopically light Fe-citrate and a heavy Fe bound to stronger chelator, and for the overall fractionation observed between substrate and cell (Wasylenki et al., 2007). It is hard to pinpoint

348 the exact fractionation mechanisms in these bio-uptake experiments as the overall fractionation
349 is resulting from FeII-FeIII redox, adsorption onto microbial biomass, possible formation of
350 thin oxyhydroxides coating, and complexation with biologically-produced Fe chelating ligands.

351 ***Bio-oxidation:*** Variations based on type of bacterial strain can be observed in Figure 2F;
352 −2.09±0.05‰ for fresh water photoautotrophs, *Thiodictyon strain F4* (Croal et al., 2004),
353 −2.94±0.05‰ for nitrate reducer *Acidovorax sp. BoFeN1* (Kappler et al., 2010), −1.99±0.24‰
354 for marine photoferrotrophs *Rhodovulum iodosum* (Swanner et al., 2015), and −3.35±0.19‰
355 for marine cyanobacterium *Synechococcus PCC7002* (Swanner et al., 2017). The precipitates
356 observed are a mixture of many FeIII oxyhydroxide phases such as ferrihydrite, goethite, and
357 lepidocrocite, where amorphous ferrihydrite was initially precipitated and then into more
358 crystalline minerals over time (Croal et al., 2004; Kappler et al., 2004 and 2010; Swanner et al.,
359 2015). A study on a natural hydrothermal spring depositing Fe oxy(hydr)oxide with and without
360 cyanobacterial biofilm showed $\Delta^{56}Fe_{sol\text{-}solid}$ of −0.54±0.08‰ (abiotic) and of −0.32±0.10‰
361 (biotic) (Mulholland et al., 2015b).

362 Kappler et al., (2010) confirmed a two-step equilibrium-kinetic microbial ferrous oxidation
363 process where equilibrium fractionation between $\Delta^{56}Fe_{FeIIaq\text{-}FeIIIaq}$ produces −3.0‰ and the
364 kinetic fractionation between $\Delta^{56}Fe_{FeIIIaq\text{-}FeIIIsolid}$ gives 1.0‰, making the final net fractionation
365 $\Delta^{56}Fe_{FeIIaq\text{-}FeIIIsolid}$ of −2.0‰ in agreement to the Rayleigh trend of −2.0‰. Swanner et al., (2017)
366 pointed out that the effect of adsorption of FeIII onto the cell surface, recovered by washing
367 with sodium acetate, $\delta^{56}Fe$ of −0.28±0.14‰ where the measured fractionation between aqueous
368 FeII and adsorbed FeIII on cell surface can produce $\Delta^{56}Fe_{FeIIaq\text{-}FeIIIacetate}$ of −1.84‰. Different
369 net $\Delta^{56}Fe_{FeIIaq\text{-}FeIIIsolid}$ observed in several experiments can be related to the proportions of
370 aqueous FeII and $FeIII(OH)_3$ precipitates at different time points, the extent of isotope exchange
371 between the two Fe pools, i.e. a combination of equilibrium which also records initial and
372 variable kinetic fractionation as well as potential changes in crystallinity of iron minerals. If Fe

isotope fractionation is induced by FeIII precipitation outside, the kinetic Fe isotope fractionation will be dominant throughout the redox cycling outside the cell in addition to equilibrium Fe isotope fractionation being dominant inside the periplasm. It is less likely that isotopic exchange will occur between aqueous Fe and $FeIII(OH)_3$ precipitate, as compared to a restricted environment of periplasm with a smaller volume of precipitates with higher surface area (Miot et al., 2009).

Bio-mineralization (MDF vs MIF): Amor et al. (2016) determined mass-dependent and mass-independent fractionation of Fe isotope during intracellular biomineralization of magnetite nanoparticles by magnetotactic bacterium, *Magnetospirillum Magneticum strain AMB-1* (Figure 2F). The magnetite is strongly enriched in light isotopes relative to initial Fe sources (FeII ascorbate and FeIII quinate) with a net fractionation of 1.39±0.19‰ for $\Delta^{56}Fe_{FeII\text{-}magnetite}$ and 2.15±0.18‰ for $\Delta^{56}Fe_{FeIII\text{-}magnetite}$. Bacterial lysate $\delta^{56}Fe$ values were enriched in the heavy isotopes relative to initial Fe sources with a net fractionation of −0.80±0.08‰ for $\Delta^{56}Fe_{FeII\text{-}Lysate}$ and −0.49±0.17‰ for $\Delta^{56}Fe_{FeIII\text{-}Lysate}$ where Fe in the lysates is more likely to be present as FeIII. Iron initially present as FeII or FeIII, was later incorporated into the cell and stored as FeIII in ferritin. FeIII was partially reduced for trafficking to magnetosomes and FeII was precipitated as magnetite in processes involving cytochromes or similar proteins. Such magnetite precipitation in AMB-1 is in line with Fe isotope fractionations determined in FeIII-reducing bacteria and in abiotic magnetite precipitation.

Mass-independent isotope fractionation (MIF) is observed in the odd isotope of Fe (^{57}Fe) but not in even isotopes (^{54}Fe, ^{56}Fe, and ^{58}Fe), highlighting a magnetic isotope effect. The initial Fe sources had $\Delta^{57}Fe$ of 0.00±0.04‰ within uncertainties and the reported mass-independent fractionation of Fe isotopes, $\Delta^{57}Fe_{FeSources\text{-}magnetite}$ ranges from 0.00‰ to -0.26‰, while the average isotope mass balance gives $\Delta^{57}Fe$ of 0.00±0.04‰, confirming isotope anomalies. The observed MIF is induced by magnetic isotope effects (MIEs) due to the nuclear spins and

nuclear magnetic moments. MIEs are usually common in reactions involving free radicals and paramagnetic species, affecting odd isotopes. As FeII is in high spin configuration and FeIII is paramagnetic, ^{57}Fe would behave differently from ^{54}Fe, ^{56}Fe, and ^{58}Fe. An extra experiment with ^{58}Fe was conducted to determine potential isotope anomalies on ^{58}Fe in comparison to ^{57}Fe; Δ^{58}Fe is ~ 0‰ within uncertainties, confirming only ^{57}Fe is affected by MIF and MIEs.

Bio-sorption: Significant Fe isotope fractionation is observed during the adsorption of FeII and FeIII onto the dead biomass of cyanobacteria (Figure 2E); *Gloeocapsa sp., Synehococcus sp., and Planthothrix sp.* (Mulholland et al., 2015b). Reported net fractionation, $\Delta^{56}Fe_{FeII\text{-}cell}$ is −1.62±0.64‰ (*Gloeocapsa sp.*), −1.97±0.12‰ (*Planthothrix sp.*) and −1.83±0.08‰ (*Synechococcus sp.*). Meanwhile, the reported $\Delta^{56}Fe_{FeIII\text{-}cell}$ is −0.65±0.17‰ (*Gloeocapsa sp.*), −0.62±0.07‰ (*Planthothrix sp.*) and −0.70±0.20‰ (*Synechococcus sp.*). The discrepancy observed between the FeII-biomass pair compared to the FeIII-biomass pair, indicates the redox state of Fe playing an important role during the adsorption. Swanner et al. (2017) have proven further that the fractionation can be as light as −2.66±0.29‰ when the adsorbed FeII is simultaneously oxidized into FeIII at the cell surface of marine cyanobacterium, *Synechococcus*. The fractionations are presumably linked to changes in Fe coordination chemistry between the aqueous phase and cells surface. The preferential enrichment of heavy isotopes on the cell surface can be due to the stronger covalent metal-ligand bonding (Fe-O-C-P) where Fe is octahedrally coordinated with phosphoryl or carboxyl groups on the cell wall, leaving behind the light isotopes of Fe aqua-complexes (O-Fe-O) in the solution.

418

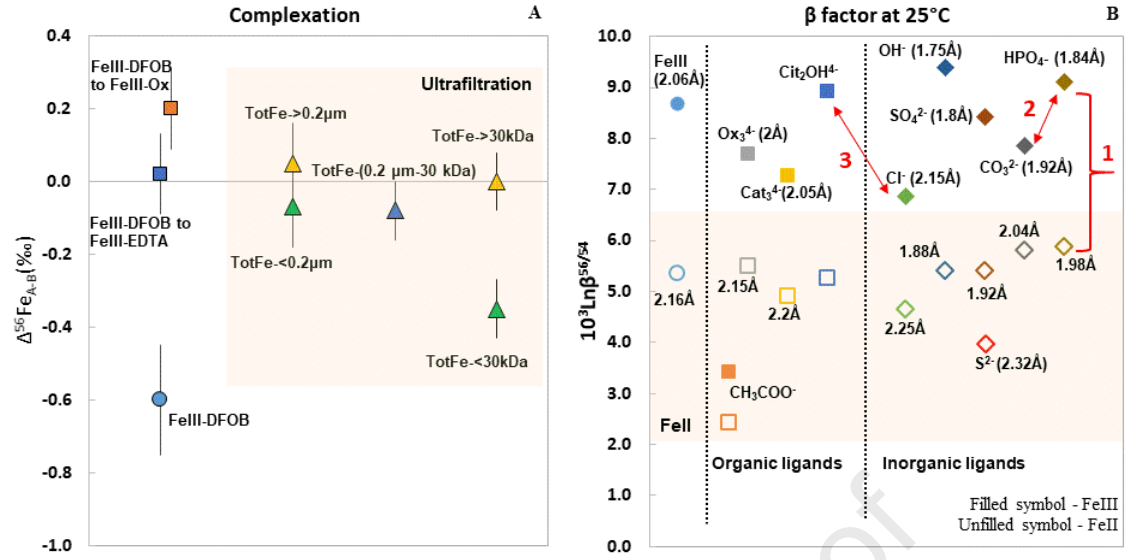

419

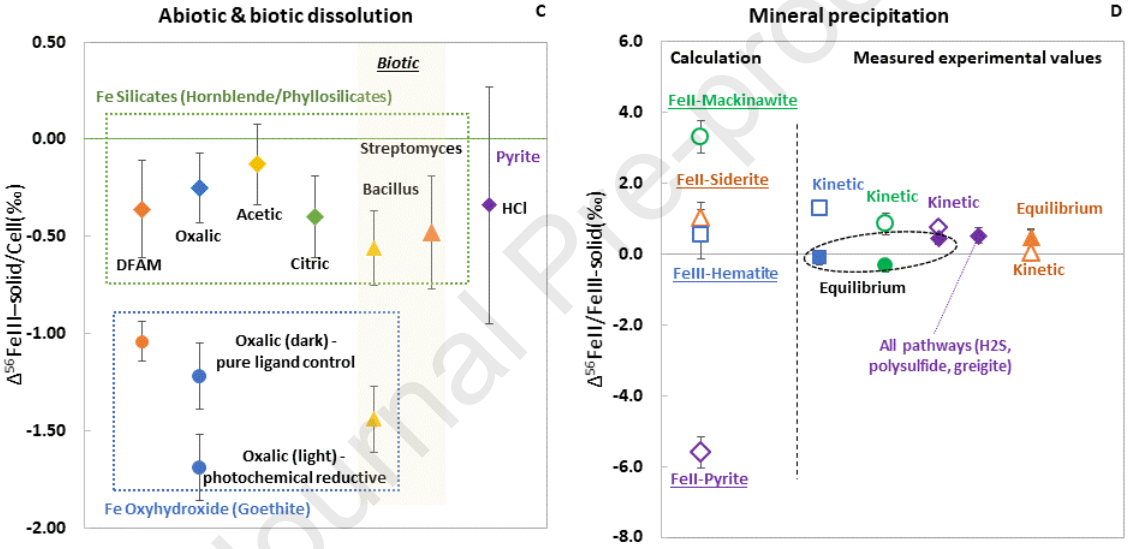

420

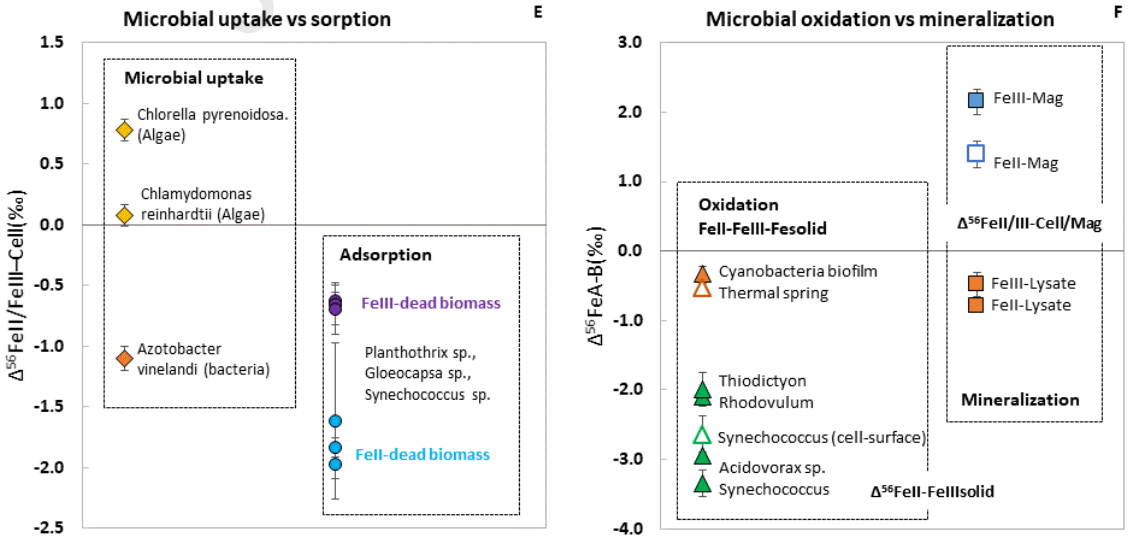

Figure 2. Iron isotope fractionation due to (A) Complexation of Fe and ligands (experimental), (B) complexation of Fe with different organic and inorganic ligands (theoretical calculation), (C) dissolution, (D) precipitation, (E) microbial uptake vs bio-sorption of FeII and FeIII onto biomass, and (F) microbial oxidation and mineralization (Mag-magnetite). In Fig (F), the green outline of one symbol in "Bio-ferrous oxidation" box corresponds to the calculation of Δ^{56}Fe between FeII-FeIII and cell surface while the rest of the calculation focused on FeII-FeIII and precipitated FeIII minerals. Error bars represent 2SD experimental replicates. Detailed values and corresponding references for Fig 2A, C, D, E, F are given in Table 2 and those for Fig 2B in Table 3.

3.6. Dissimilatory iron reduction (abiotic vs biotic)

Iron reducing microorganisms complete the iron redox cycle by dissimilative reduction of FeIII to FeII in neutrophilic environments under anaerobic conditions. Microorganisms from both the Archaea and Bacteria domains are capable of metabolically exploiting the favorable redox potential of iron. They respire FeIII as its terminal electron acceptor coupled to oxidation of organic carbon/hydrogen into assimilation of biomass. Several studies have confirmed Fe isotope fractionation during dissimilatory reduction of Fe minerals such as goethite, hematite, ferrihydrite, magnetite, siderite by both strictly anaerobic bacterium, *Geobacter* and facultative anaerobic bacterium, *Shewanella* species. There are three different types of fractionation reported in these studies (1) equilibrium fractionation between aqueous FeII and bulk goethite, (2) fractionation between aqueous FeII and sorbed FeII, and (3) fractionation between aqueous FeII and reactive FeIII in the solid surface. These studies have concluded that Fe isotope fractionation was largely driven by electron and atom exchange between $FeII_{aq}$ and a reactive FeIII layer ($FeIII_{reac}$) produced on the Fe mineral surface.

Coupled electron transfer-atom exchange at the iron mineral surface is described in three consecutive steps: (1) adsorption of $FeII_{aq}$ onto FeIII mineral surface, (2) the electron transfer

446 from the adsorbed FeII into the structural FeIII of iron mineral, followed by the atom-exchange
447 between the two, and (3) the subsequent release of FeII from the ferric structure into the solution
448 (Mikutta et al., 2009).

449 Adsorption

450 $$[{}^{k}Fe(II)]_{aq} + 2{}^{i}Fe(III)OH \leftrightarrow \equiv \left({}^{i}Fe(III)O\right)_2 {}^{k}Fe(II) + 2[H^+]_{aq}$$

451 Electron transfer

452 $$\equiv \left({}^{i}Fe(III)O\right)_2 {}^{k}Fe(II) + \equiv {}^{i}Fe(III)OH \leftrightarrow \equiv \left({}^{i}Fe(III)O\right)_2 {}^{k}Fe(III) + \equiv {}^{i}Fe(II)OH$$

453 Desorption

454 $$\equiv {}^{i}Fe(II)OH \leftrightarrow \left[{}^{i}Fe(II)\right]_{aq} + [OH^-]_{aq}$$

455 where subscripts denote different isotopes of Fe where i > k (e.g., i = ^{56}Fe, k = ^{54}Fe)

456 ***Dissimilatory iron reduction of goethite:*** The reported fractionation between the $FeII_{aq}$ and
457 bulk goethite, $\Delta^{56}Fe_{FeIIaq\text{-}goethite}$ ranges from −0.52‰ to −1.61‰ (average of −0.89±0.33‰) in
458 presence of *Shewanella putrefaciens* and *Geobacter sulfurreducens* (Crosby et al., 2005 &
459 2007; Icopini et al., 2004). In parallel abiotic experiments, $FeII_{aq}$ adsorption onto goethite
460 shifted $\Delta^{56}Fe_{FeIIaq\text{-}goethite}$ by −0.80‰ (Icopini et al., 2004). Similarly, different particle size of
461 goethite could also affect the overall fractionation, $\Delta^{56}Fe_{FeIIaq\text{-}goethite}$ as −1.05±0.08‰ for micro-
462 goethite and −1.22±0.08‰ for nano-goethite (Beard et al., 2010; Frierdich et al., 2014a, Reddy
463 et al., 2015).

464 Fractionation between aqueous and sorbed FeII, $\Delta^{56}Fe_{FeIIaq\text{-}FeIIsorbed}$ ranges from −0.58‰ to
465 −1.18‰ for *Shewanella putrefaciens* and *Geobacter sulfurreducens* (average −0.86±0.18‰,
466 Crosby et al., 2005 & 2007). However, no significant difference is observed between nano and
467 micro-goethite, with $\Delta^{56}Fe_{FeIIaq\text{-}FeIIsorbed}$ of −1.24±0.14‰ in abiotic experiment (Beard et al.,
468 2010). Greater quantities of FeII are sorbed to nano-goethite relative to micro-goethite due to

larger surface area, with maximum sorption at pH 6.5-7.5 and minimum at lower pH, effecting the initial kinetic isotope effects (Beard et al., 2010; Reddy et al., 2015). Over time, these variable kinetic isotope fractionation merged slowly towards the equilibrium $Fe(II)_{aq}$-goethite fractionation (Frierdich et al., 2014a).

Fractionation between $FeII_{aq}$ and surface reactive FeIII or "$FeIII_{reac}$", $\Delta^{56}Fe_{FeIIaq\text{-}FeIIIreac}$ ranges from −2.49‰ to −3.89‰ for *Shewanella putrefaciens* and *Geobacter sulfurreducens,* where the average is −2.62±0.64‰ (Crosby et al., 2005 & 2007). Beard et al. (2010) also reported significant fractionation, $\Delta^{56}Fe_{FeIIaq\text{-}FeIIIreac}$ as −1.68±0.08‰ for micro-goethite and −2.10±0.48‰ for nano-goethite. The overall isotopic fractionation $FeII_{aq}$ and $FeIII_{reac}$ should be ~ −3.0‰ if it reflects equilibrium fractionation at room temperature.

Jang et al. (2008) claimed that isotopic composition of $FeII_{aq}$ is largely controlled by sorption of FeII onto goethite and there is a kinetic fractionation associated with electron transfer from adsorbed FeII to structural FeIII of goethite, producing FeIII with higher δFe than $FeII_{aq}$ and initial goethite. Different particle size can also further contribute to the difference in surface area, crystal edges, corners or faces creating different energetic sites hosting $FeIII_{reac}$.

Dissimilatory iron reduction of hematite: The reported fractionation between the $FeII_{aq}$ and bulk hematite, $\Delta^{56}Fe_{FeIIaq\text{-}hematite}$ is ranging from −0.97‰ to −2.07‰ for *Shewanella putrefaciens* and *Geobacter sulfurreducens* (average –1.56±0.28‰, Crosby et al., 2005 & 2007). Frierdich et al. (2014b & 2015) confirmed Fe isotope exchange was a function of particle size using an enriched ^{57}Fe-tracer in a parallel abiotic experiment. Experimental $\Delta^{56}Fe_{FeIIaq\text{-}hematite}$ ranges from −2.77±0.37‰ for fine-grained hematite (60 m^2g^{-1}) to −3.1±0.36‰ coarse-grained hematite (7 m^2g^{-1}) (average −2.83±0.25‰, Frierdich et al., 2019).

The reported fractionation between the $FeII_{aq}$ and sorbed FeII, $\Delta^{56}Fe_{FeIIaq\text{-}FeIIsorbed}$ ranges from −0.07‰ to −0.53‰ for both bacteria strains (average −0.30±0.15‰, Crosby et al., 2005 & 2007). A similar fractionation of −0.48±0.07‰ is observed in experiment without Si, at pH

494 7 and it shifted to −0.20±0.13‰ with Si (Wu et al., 2009). Formation of Fe-Si gel was reported
495 at pH 8.7 where the fractionation between $FeII_{aq}$ and Fe-Si gel, $\Delta^{56}Fe_{FeIIaq\text{-}FeIISiGel}$ is
496 −0.51±0.18‰, which is indistinguishable from the average fractionation, $\Delta^{56}Fe_{FeIIaq\text{-}FeIIsorbed}$ at
497 pH 7. In a parallel abiotic experiment, $\Delta^{56}Fe_{FeIIaq\text{-}FeIIsorbed}$ ranges from −0.74±0.45‰ for fine-
498 grained hematite (60 m^2g^{-1}) to −0.83±1.08‰ for coarse-grained hematite (7 m^2g^{-1}) (reported
499 average −0.77±0.17‰ for all particle size, Frierdich et al., 2019).

500 A larger range of $\Delta^{56}Fe_{FeIIaq\text{-}FeIIIreac}$ is reported; −2.51‰ to −4.01‰ for both bacteria strains
501 (average −2.95±0.19‰, Crosby et al., 2005 & 2007), comparable to −2.64±0.19‰ without Si
502 at pH 7 (Wu et al., 2009). Presence of dissolved Si could favor the heavy isotopic signature of
503 surface reactive FeIII, for example, the average fractionation $\Delta^{56}Fe_{FeIIaq\text{-}FeIIIreac}$ is −1.90±0.47‰
504 with Si at pH 7 and −2.64±0.19‰ without Si at pH 7. However, higher pH could favor light
505 signature in surface reactive FeIII even in the presence of Si (average −2.66±0.18‰ with Si at
506 pH 8.7 and −1.76±0.21‰ without Si, at pH 8.7). At elevated pH (8.7) the hematite reduction
507 by *G. sulfurreducens,* reduced the size of the total reactive Fe pool and FeII existed exclusively
508 as sorbed FeII (Wu et al., 2009).

509 Although kinetic effect could occur during rapid sorption of FeII onto hematite,
510 recrystallization of hematite will govern the overall fractionation process. If homogeneous
511 recrystallization occurs, where the mineral continuously equilibrates with the fluid, the isotopic
512 values of $FeII_{aq}$ linearly will approach steady state, depicting equilibrium fractionation. If
513 heterogeneous recrystallization occurs, where portion of the mineral no longer interacts with
514 the fluid due to FeII oxidative growth, the isotopic composition of $FeII_{aq}$ will approach the same
515 value as hematite, in apparent violation of equilibrium fractionation effect (Frierdich et al.,
516 2019).

517 ***Goethite vs Hematite vs particle sizes:*** Particle size dependent Fe isotope fractionation is
518 observed during the interaction between $FeII_{aq}$ and goethite, as well as $FeII_{aq}$ and hematite. In

general, $\Delta^{56}Fe_{FeIIaq\text{-}goethite}$ is more negative for smaller particle size, whereas the opposite trend is observed for $\Delta^{56}Fe_{FeIIaq\text{-}hematite}$ with more positive values. Difference between fractionation for nano- and micro-goethite is 0.2‰ compared to that between nano- and micro-hematite which is 0.5‰. Therefore, the effect of particle size is more visible on the extent of isotopic exchange between $FeII_{aq}$ and hematite than in goethite. Larger Fe isotope fractionation in smaller particle size of goethite could reflect a higher proportion of surface atoms that preferentially concentrate the heavy Fe isotopes in high energy surface bonds (Beard et al., 2010; Frierdich et al., 2014a). However, the opposite trend of larger Fe isotope fractionation in large particle sizes of hematite could indicate different fractionation mechanisms. If kinetic isotope fractionation were the governing process, light isotopes of Fe can be expected to preferentially partition into hematite during rapid sorption, leaving a heavy isotopic signature in aqueous FeII. However, the opposite trend of light isotopic signature in aqueous FeII rules out the kinetic isotope effect.

Dissimilatory iron reduction of ferrihydrite: Hydrous ferric oxide (HFO or ferrihydrite) is quickly precipitated in neutral environments, making it widespread in soils and sediments. Fractionation between the $FeII_{aq}$ and bulk ferrihydrite, $\Delta^{56}Fe_{FeIIaq\text{-}ferrihydrite}$ is −1.30±0.22‰ in the presence of *Shewanella alga* (*Strain BrY and Strain BCMB,* given in Figure 3C) where the fractionation is invariant with the choice of growth media and strains (Beard et al., 1999 & 2003). In parallel, in abiotic studies, the reported equilibrium fractionation between $FeII_{aq}$ and pure HFO without impurities, $\Delta^{56}Fe_{FeIIaq\text{-}HFO}$ is −3.2±0.10‰. When dissolved Si is present, $\Delta^{56}Fe_{FeIIaq\text{-}HFO+Si}$ is −3.17±0.08‰. However, it is completely shifted if Si is coprecipitated with HFO, thereby embedded inside the HFO structure (molar Si:Fe =1), with $\Delta^{56}Fe_{FeIIaq\text{-}Si\text{-}HFO}$ of −2.58±0.14‰ (Wu et al., 2011). Similarly, when HFO is coprecipitated with Suwannee River natural organic matter (SRNOM, molar C:Fe=1.2), the reported equilibrium fractionation,

543 $\Delta^{56}Fe_{FeIIaq\text{-}C\text{-}HFO}$ is −2.36±0.26‰ (Chanda et al., 2020). Unfortunately, there is no data available
544 for the estimated equilibrium $\Delta^{56}Fe_{FeII\text{-}ferrihydrite}$ using β factor.

545 It has been difficult to determine equilibrium Fe isotope fractionation between aqueous FeII
546 and HFO due to the fast transformation of the latter to more stable minerals (Wu et al., 2011).
547 The presence of C and Si in ferrihydrite structure could inhibit the rapid transformation of
548 ferrihydrite to more stable iron oxides upon interaction with aqueous FeII (Chanda et al., 2020).
549 The presence of C and Si also increased the extent of Fe isotope exchange, shifting the overall
550 fractionation. Dissolved Si could block the reactive surface sites by sorption via inner-sphere
551 complexes, inhibiting atom exchange between FeII and FeIII of HFO. Liberation of Si from Si-
552 HFO coprecipitate into solution presumably freed reactive surface sites, thus promoting
553 isotopic exchange between FeII and the Si-HFO coprecipitate. Si mass transfer from Si-HFO
554 into solution was accompanied by Fe transfer from aqueous $FeII_{aq}$ into Si-HFO solid,
555 facilitating both electron transfer as well as atom exchange. Similarly, coprecipitation with
556 organic C changes Fe bonding environment, where the coordination number of Fe-Fe bonds in
557 FeO_6 octahedral structure decreases along with the decline in crystal size, resulting in increased
558 numbers of defects and a more disordered surface, in turn influencing the equilibrium
559 fractionation factor (Wang et al., 2016, Zhou et al., 2018; Chanda et al., 2020).

560 ***Dissimilatory iron reduction of siderite:*** Johnson et al. (2005) conducted a study on
561 biogenic siderite formation via dissimilatory reduction of hydrous ferric oxides by *Geobacter*
562 *sulfurreducens*, where the estimated equilibrium fractionation between $FeII_{aq}$ and siderite,
563 $\Delta^{56}Fe_{FeIIaq\text{-}siderite}$ is 0.0±0.22‰, near zero for pure siderite and ~1‰ for Ca-substituted siderite
564 (Figure 3C). Kinetic isotope effects are responsible for large fractionation observed in an initial
565 period, where $\Delta^{56}Fe_{FeIIaq\text{-}siderite}$ can be as large as 1.2‰ for pure siderite and 2.2‰ for Ca-
566 substituted siderite. Wiesli et al. (2004) have assessed the equilibrium fractionation factor
567 between $FeII_{aq}$ and siderite by performing abiotic experiments where the reported

568 $\Delta^{56}Fe_{FeIIaq\text{-}siderite}$ at 20°C is 0.48±0.22‰ based on slow carbonate precipitation experiments. No
569 discernable isotopic fractionation was observed at extremely rapid synthesis of siderite (a few
570 seconds). Johnson et al. (2003) initially predicted $FeII_{aq}$ and siderite fractionation to lie in the
571 range of −1.7‰ to 0.3‰ at 25°C. The net fractionation increases with decreasing mole fraction
572 of Fe from siderite to ankerite, indicating carbonate stoichiometry exerting a substantial control
573 on Fe isotope fractionations. Bonding changes and distortions in the crystal lattice due to Ca
574 substitution in siderite could be the reason behind such large Fe isotope effects, a similar
575 fractionation could be expected in Mn and Mg substitution.

576 ***Dissimilatory iron reduction of magnetite:*** Magnetite is well-known for housing both
577 redox species of Fe; one FeIII ion on the tetrahedral site (A site), and one FeII and one FeIII
578 ion on the octahedral site (B site), posing great challenge for experimental studies. Johnson et
579 al. (2005) estimated fractionation between $FeII_{aq}$ and magnetite, $\Delta^{56}Fe_{FeIIaq\text{-}magnetite}$ is
580 −1.34±0.22‰ from magnetite precipitation during microbial Fe reduction of ferrihydrite by
581 *Geobacter sulfurreducens* (Figure 3D). Frierdich et al. (2014b) conducted abiotic experiment
582 using ^{57}Fe enriched tracer, three-isotope method and multi-directional approach to equilibrium.
583 The extrapolated equilibrium fractionation between $FeII_{aq}$ and magnetite, $\Delta^{56}Fe_{FeIIaq\text{-}magnetite}$ is
584 −1.56±0.22‰ at 22°C regardless of distinct initial isotope signatures. An additional experiment
585 was conducted to study the effect of phase transformation on Fe isotope exchange during
586 magnetite synthese by reacting $FeII_{aq}$ and ferrihydrite, with final $\Delta^{56}Fe_{FeIIaq\text{-}magnetite}$ of
587 −1.61±0.22‰, identical within errors to other experiments. It is also relevant to compare the
588 intracellular biomineralization of magnetite nanoparticles by *Magnetospirillum Magneticum*
589 *strain AMB-1,* inducing a much higher $\Delta^{56}Fe_{FeIIsubstrate\text{-}magnetite}$ of 1.39±0.19‰ (Amor et al.,
590 2016, See the details in section 3.4).

591 Fe isotope exchange between $FeII_{aq}$ and magnetite could reflect two possible mechanisms
592 (i) an initial kinetic isotope effects during rapid dissolution and reprecipitation (ii) site-specific

593 isotope exchange such as octahedral vs. tetrahedral sites (Frierdich et al., 2014b). Relative
594 heavy $\delta^{56}Fe$ of $FeII_{aq}$ reflect the kinetic isotope transport where light $FeII_{aq}$ being transferred
595 via boundary layer and attaching to the magnetite surface, kinetic isotope effects were later
596 erased by an approach to equilibrium at greater extents of exchange. One third of Fe in
597 magnetite bound as FeIII in tetrahedral site (A site) and two thirds of Fe bound as FeII+FeIII
598 in octahedral site (B site). Based on the different β factors available for each site in magnetite
599 ($10^3 Ln\beta^{56/54}_{SiteA}$ as 7.5‰ and $10^3 Ln\beta^{56/54}_{SiteB}$ as 5.7‰[6]), calculated tetrahedral site A hosting
600 FeIII should have $^{56}Fe/^{54}Fe$ ratio 1.8‰[7] higher at 25°C (Personal communication and Polyakov
601 et al., 2007). Isotope selective exchange experiment and Mössbauer spectroscopy by Gorski et
602 al. (2012) showed no indication of preferential exchange of Fe isotope based on tetrahedral or
603 octahedral site.

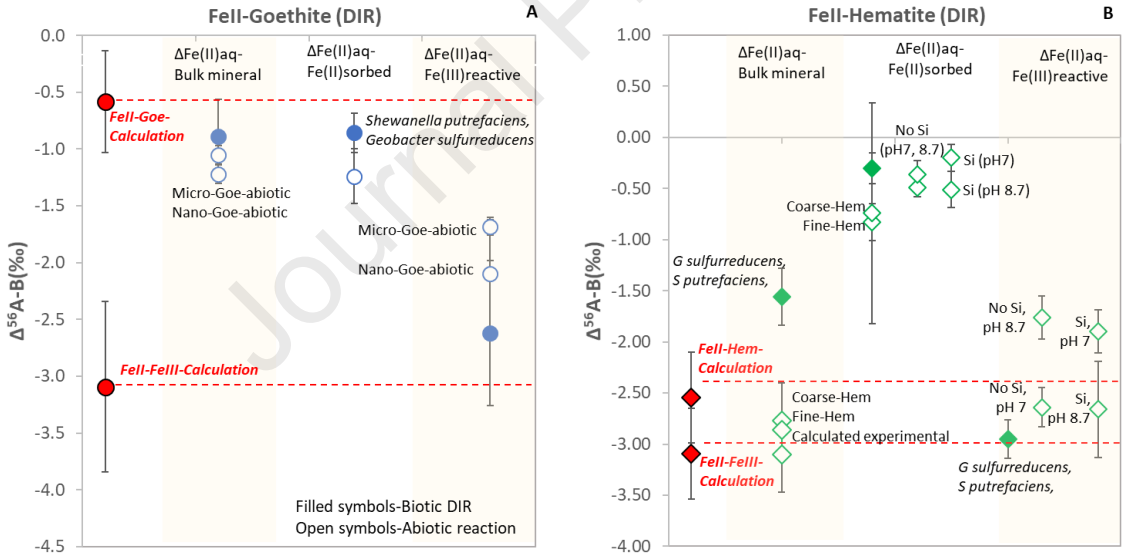

604

[6] Via personal communication, updated polynomial coefficients of $^{57/54}Fe$ for magnetite :
$10^3 ln\beta A = 1.0168\ X - 2.946 \times 10^{-3}\ X^2 + 1.2032 \times 10^{-5}\ X^3$
$10^3 ln\beta B = 0.7668\ X - 1.678 \times 10^{-3}\ X^2 + 5.3232 \times 10^{-6}\ X^3$
$10^3 ln\beta = 0.8502\ X - 2.101 \times 10^{-3}\ X^2 + 7.5595 \times 10^{-6}\ X^3$
Conversion to $10^3 ln\beta^{56/54}Fe$, multiply $10^3 ln\beta^{57/54}Fe$ by (2/3)*(57/56)

[7] Previous reported value is 3.5‰ as reported by Frierdich et al., 2014b using erroneous β factors of Polyakov and Mineev(2000).

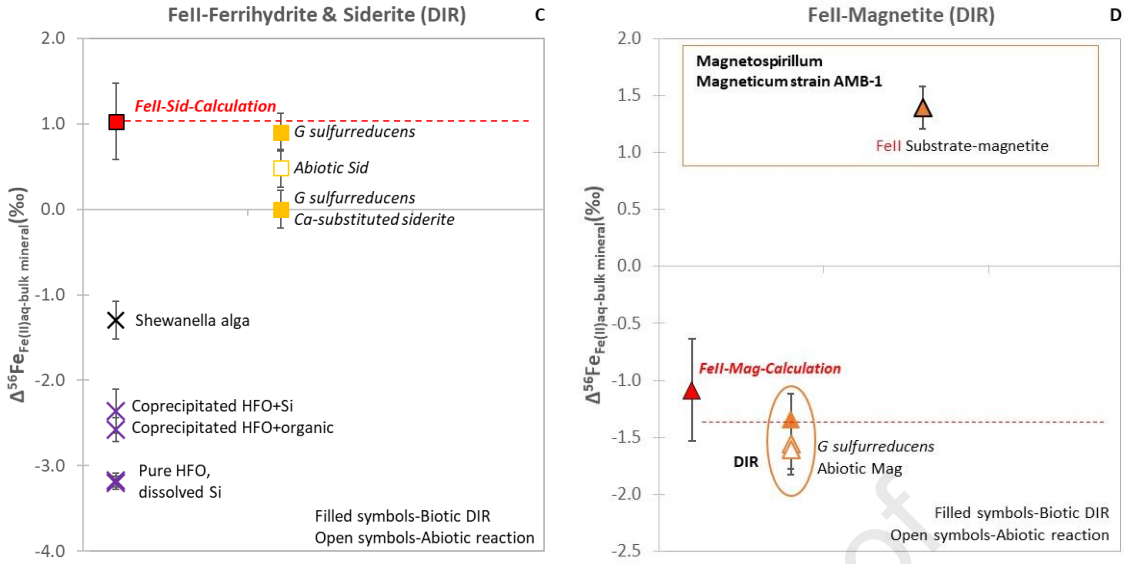

Figure 3. Dissimilatory iron reduction processes or microbial iron reduction of (A) Goethite, (B) Hematite, (C) Ferrihydrite and Siderite, (D) Magnetite in comparison to abiotic reduction reaction and available calculation data. Error bars represent 2SD experimental replicates.

4. Comparison between experimental studies and theoretical ones

In parallel to several experimental studies, spectroscopy studies and pure theoretical calculations were done to determine reduced partition function ratios (β factor) in order to evaluate the equilibrium fractionation factors of iron isotopes, $10^3 Ln\beta^{56/54}$. Mössbauer spectroscopy and inelastic nuclear resonant X-ray scattering (INRXS) in synchrotron radiation experiments were used to investigate β factor of different iron minerals (Polyakov and Mineev, 2000; Polyakov et al., 2007; Polyakov and Soultanov., 2011; Polyakov et al., 2013). Density functional theory (DFT) and ab-initio calculations were applied to determine the β factor of iron with different organic and inorganic species in aquatic media (Anbar et al., 2005; Domagal-Goldman and Kubicki, 2008; Hill et al., 2009; Ottonello and Zuccolini, 2009; Fujii et al., 2014). For example, the equilibrium iron isotope fractionation due to redox reaction between FeII and FeIII can be calculated using the β factor ($10^3 Ln\beta^{56/54}$) obtained from the study of Fujii et al. (2014) and is given in Table 1.

$$10^3Ln\alpha^{56/54}_{FeII\text{-}FeIII} = 10^3Ln\beta^{56/54}_{FeII} - 10^3Ln\beta^{56/54}_{FeIII} = 5.10 - 8.07 = -2.98‰$$

The calculated $10^3Ln\alpha^{56/54}_{FeII\text{-}FeIII}$ varies up to 0.75‰ depending on the variations of the individual $10^3Ln\beta^{56/54}_{FeII}$ and $10^3Ln\beta^{56/54}_{FeIII}$ from different studies (Table 1). Different equilibrium fractionation factors, $10^3Ln\alpha^{56/54}_{A\text{-}B}$, for each biogeochemical process are calculated and given in Table 2 in order to compare with the values obtained in experimental studies. During redox reactions, the average $10^3Ln\alpha^{56/54}_{FeII\text{-}FeIII}$ obtained using the reduced partition function ratios (β factor) is −3.09±0.75‰, in agreement with the equilibrium experimental values, $\Delta^{56}Fe_{FeII\text{-}FeIII}$: −3.00±0.23‰ obtained in experimental studies (Johnson et al., 2002; Welch et al., 2003).

Precipitation: the experimental equilibrium fractionation during hematite precipitation remains close to zero ($\Delta^{56}Fe_{III\text{-}Hematite\_Equilibrium}$ −0.15±0.20‰ at 25°C) while it was estimated at 0.29±0.70‰ from Mössbauer spectroscopy studies and density functional theory (Fujii et al., 2014 & Polyakov et al., 2007). Similarly, the experimental equilibrium fractionation factor between FeII and siderite, $\Delta^{56}Fe_{II\text{-}Siderite\_Equilibrium}$ of 0.48±0.22‰, is smaller than the theoretical prediction, $10^3Ln^{56}\alpha_{FeII\text{-}Siderite}$ of 0.89±0.45‰ (Fujii et al., 2014 and Blanchard et al., 2009). Using very old spectroscopic data for Mackinawite led to great uncertainties and huge discrepancy where a much larger fractionation, $10^3Ln^{56}\alpha_{FeII\text{-}Mackinawite}$ of 3.17±0.45‰ (Fujii et al., 2014; Polyakov and Soultanov., 2011) is predicted in comparison to the experimental values, $\Delta^{56}Fe_{II\text{-}Mackinawite\_Equilibrium}$ of −0.33±0.16‰ (Butler et al., 2005; Guilbaud et al., 2010; Guilbaud et al., 2011a). In Pyrite precipitation, predicted equilibrium isotopic fractionation between $FeII_{aq}$ and pyrite[8], $10^3Ln^{56}\alpha_{FeIIaq\text{-}Pyrite}$ is −5.74‰ (Fujii et al., 2014; Polyakov and Soultanov, 2011), is significantly different from the experimental fractionation factor, $\Delta^{56}Fe_{II\text{-}Pyrite\_Equilibrium}$ 0.44±0.15‰ (Mansor and Fantle et al., 2019).

[8] please note that only β factor of pyrite from Polyakov and Soultanov, (2011) is only considered due to experimental validation in conjunction with sulfur isotopes.

Bio-oxidation and Bio-mineralization: During the microbial oxidation of FeII to FeIII, the oxidized FeIII precipitated into a mixture of FeIII minerals such as ferrihydrite, goethite, and lepidocrocite. The experimental fractionation between FeII-FeIII$_{solids}$, $\Delta^{56}Fe_{FeII\text{-}FeIII\text{-}FeIIISolid}$ varies for each bacteria strain as seen in Table 2. Nonetheless, these experimental values can be further compared to the estimated $10^3Ln^{56}\alpha_{A\text{-}B}$ between FeII, FeIII, goethite and lepidocrocite initially proposed by Beard and Johnson (2004), Johnson et al. (2005), and Dauphas and Rouxel (2006) as follows:

$$\Delta^{56}Fe_{FeIIaq\text{-}FeIIIsolid} \rightarrow \Delta^{56}Fe_{FeIIaq\text{-}FeIIIaq} + \Delta^{56}Fe_{FeIIIaq\text{-}FeIIIsolid}$$

The calculated $10^3Ln^{56}\alpha_{A\text{-}B}$ on FeII-FeIII-minerals deviated from experimental values, with a smaller net value of <1‰ ($10^3Ln^{56}\alpha_{FeII\text{-}FeIII\text{-}Goethite}$ −0.72‰ for FeII-FeIII-Goethite and $10^3Ln^{56}\alpha_{FeII\text{-}FeIII\text{-}lepidocrocite}$ −0.34‰ for FeII-FeIII-lepidocrocite). The more negative values (−1.99‰ and −3.35‰ in Table 2) observed for $\Delta^{56}Fe_{FeII\text{-}FeIIaq\text{-}FeIIIsolid}$ in experimental studies could be related to several possible mechanisms: (1) equilibrium exchange between FeII and FeIII species, (2) additional equilibrium isotope shift control by bioligands, (3) formation of a mixture of final FeIII oxyhydroxide minerals (ferrihydrite, goethite, lepidocrocite) and their subsequent transformation of one mineral to another, (4) similar colloidal Fe phases bound to additional inorganic ligands (SiO_4^{4-} and PO_4^{4-}), (5) a kinetic isotope effect produced by such precipitation over the equilibrium exchange between existing Fe species and inorganic/organic ligands, (6) difference in specific surface area of bacteria (Synechococcus cyanobacteria vs Rhodovulum) to sorb iron, favoring additional isotope shift, and (7) specific metabolic pathway of each microbial strain, for instance, FeII oxidation by *Acidovorax sp.* strain taking place in the periplasm where equilibrium is attained via coupled electron and atom exchange between FeIIaq and FeIIIprecipitates in the periplasm.

During intracellular biomineralization of magnetite nanoparticles by *Magnetospirillum Magneticum strain AMB-1*, the net equilibrium isotopic fractionation $\Delta^{56}Fe_{FeII\text{-}magnetite}$(‰) is

1.39±0.19‰ and $\Delta^{56}Fe_{FeIII\text{-}magnetite}$(‰) is 2.15±0.18‰ (Amor et al., 2016). A much closer equilibrium isotopic fractionation is calculated for $10^3Ln^{56}\alpha_{FeIII\text{-}magnetite}$(‰), 1.75±0.70‰ compared to $10^3Ln^{56}\alpha_{FeII\text{-}magnetite}$(‰), −1.22±0.45‰ (Fujii et al., 2014; Polyakov, personal communication, 2020).

Dissimilatory iron reduction: During the microbial reduction of goethite, the predicted equilibrium isotope fractionation, $10^3Ln^{56}\alpha_{FeII\text{-}Goethite}$ is −0.72±0.45‰ (Fujii et al., 2014; Polyakov & Mineev., 2000), in agreement with fractionation obtained from biotic experiment, $\Delta^{56}Fe_{FeIIaq\text{-}Goethite}$ of −0.89±0.33‰ (Crosby et al., 2005 & 2007; Icopini et al., 2004), given in Table 4. However, it is slightly higher than the abiotic experimental fractionation factors; −1.05±0.08‰ for micro-goethite and −1.22±0.08‰ nano-goethite (Beard et al., 2010; Frierdich et al., 2014; Reddy et al., 2015). The Beard et al. (2010) extrapolated $\Delta^{56}Fe_{FeIII\text{-}Hematite}$(‰) from the study of Skulan et al. (2002)[9] to a temperature of 20°C to be −0.15‰. In combination with the study of Welch et al. (2003) where $\Delta^{56}Fe_{FeII\text{-}FeIII}$(‰) is −3.01‰, the calculated experimental $\Delta^{56}Fe_{FeII\text{-}hematite}$(‰) between relevant experimental studies is −2.86‰ in a very close vicinity to the values obtained by Frierdich et al. (2019). In comparison, the direct estimated equilibrium $10^3Ln^{56}\alpha_{FeII\text{-}Hematite}$(‰) obtained from β factors of $[FeII(H_2O)_6]^{2+}$ and hematite; −2.68‰ which is slightly lower (Fujii et al., 2014; Polyakov et al., 2007). Theoretical predictions obtained the equilibrium fractionation, $10^3Ln^{56}\alpha_{FeII\text{-}Pyrite}$(‰) of 0.89‰ (Blanchard et al., 2009; Rustad et al., 2010; Fujii et al., 2014), a much closer values to the experimental values, $\Delta^{56}Fe_{FeII\text{-}Pyrite}$(‰) of 1.00±0.22‰ obtained in Ca-substituted siderite (Johnson et al., 2005). In comparison, the predicted equilibrium factor, $10^3Ln^{56}\alpha_{FeIIaq\text{-}magnetite}$(‰) is −1.22±0.45‰ (Fujii et al., 2014; Polyakov, personal communication, 2021), lower than the equilibrium experimental values.

Discrepancy between experimental fractionation and theoretical predictions: It is important to reconcile the discrepancies and inconsistencies observed between predicted and

[9] Skulan et al. (2002) initially conducted the experiment at 98°C, the measured fractionation is −0.10‰.

694 experimentally determined equilibrium fractionation factors. The main issue in comparison is
695 that calculation can be accounted for single step or simple process while several processes can
696 take place simultaneously in experimental studies which resulted in fractionation. It is hard to
697 constrain Fe reactivity experimentally in order to isolate specific processes and to decipher
698 respective fractionation.

699 It is possible to estimate the extent of discrepancy between experimental and theoretical
700 values especially for redox reactions by considering all absolute values obtained and the
701 respective standard deviation: the estimated discrepancy range is between 0.43‰ to 0.61‰.
702 The type of model (gas vs aqueous) used for the calculations (some theoretical studies ignoring
703 the effects of extended hydration spheres), the experimental design/set-up (iron speciation such
704 as nitrate, chloride, salinity, temperature), final iron separation and recovery, experimental
705 artifacts (formation of unwanted colloids), kinetic isotope effect on the determined final
706 equilibrium fractionation, mathematical methods of calculation and overall analytical
707 uncertainties, these could all be accounted for the discrepancy estimated between experimental
708 and theoretical values in the case of redox reactions.

709 The theoretical vs experimental comparison is harder to do for biogeochemical processes
710 other than redox reactions, due to fractionation values that envelop several complexities in the
711 experimental studies, while seeming over-simplified in theoretical ones. For instance, in
712 hematite precipitation experiment (Table 4), the kinetic isotope effect between FeIII and
713 hematite is significantly much bigger than the equilibrium isotope effect, while the theoretical
714 calculation failed to distinguish between the two. The limitation in theoretical studies is due to
715 the type of model used as mentioned before, as well as to the purity, age, particle size,
716 crystallinity of the minerals modelled, and for in spectroscopy studies it is mainly due to
717 analytical uncertainties. Likewise, several complexities in the experiments include the diverse
718 formation pathways of iron minerals (as in redox reactions), their sensitivity to pH and

719 temperature changes, their crystallinity and stability, the incorporation of impurities, the
720 bonding environment, the influence of biological factors (bio-uptake, bio-sorption, their
721 different metabolic pathways, the complexation with several metabolites and bio-products).
722 Despite how arbitrary it could seem to be, we estimate the discrepancy range between iron
723 fractionation determined experimentally vs theoretically: it lies between 0.43‰ and 1.59‰ for
724 kinetic fractionation and between -0.94‰ and 0.06‰ for equilibrium fractionation.

725 It is also possible that one or more geochemical processes can take place at the same time
726 such as dissolution and recrystallization, and formation of thin mineral crust and subsequent
727 adsorption, which could modify the Fe isotope signatures and will add more complexity to the
728 matter. Therefore, predicted equilibrium isotope fractionation from theoretical calculation or
729 spectroscopy studies does not account for such issues. Nonetheless, it is reliable and consistent
730 to compare predicted and observed equilibrium fractionations between fluid–fluid or mineral–
731 mineral fractionations, rather than for fluid–mineral fractionations.

732

733

734 Table 1. Reduced partition function ratios (β factor-$10^3 Ln\beta^{56/54}$) obtained in spectroscopy
735 studies and theoretical calculations for different iron minerals vs redox Fe species (FeII and
736 FeIII). The Schauble et al. (2001) calculation is not considered because the $10^3 Ln\beta^{56/54}$FeIII is
737 a significant outlier due to spectroscopic data issues.

References	**Iron minerals**	**$10^3 Ln\beta^{56/54}$ at 25°C**
Polyakov and Mineev, 2000	Goethite	5.82
	Lepidocrocite	5.44
Polyakov et al., 2007	Hematite	7.78
Polyakov & Soultanov., 2011	Pyrite	10.84
Polyakov & Soultanov., 2011	Mackinawite	1.92
Blanchard et al., 2009	Siderite	4.20
Polyakov (personal communication)	Magnetite	6.32
References	**$10^3 Ln\beta^{56/54}$ for $[FeII(H_2O)_6]^{2+}$**	**$10^3 Ln\beta^{56/54}$ for $[FeIII(H_2O)_6]^{3+}$**
Anbar et al., 2005	5.69	8.75
Domagal-Goldman & Kubicki., 2008	5.77	8.62
Ottonello & Zuccolini., 2009	4.86	9.33
Rustad et al., 2010	4.66	7.69
Moynier et al., 2013	5.32	7.50
Fujii et al., 2014	5.10	8.07

738

739 Table 2. Comparison of the equilibrium iron isotope fractionation obtained in experimental
740 studies ($\Delta^{56}Fe_{A-B}$) to those obtained in spectroscopy studies and theoretical calculations
741 ($10^3Ln\beta^{56/54}$) for redox reactions, complexation, dissolution, precipitation, bio-oxidation, bio-
742 mineralization.

References	Fe Pairs	Scope of studies	$\Delta^{56}Fe_{A-B}$(‰)
Redox Equilibriation			
Johnson et al., 2002; Welch et al., 2003	Abiotic FeII-FeIII	$\Delta^{56}Fe_{FeII-FeIII}$	-3.00 ± 0.23‰
Anbar et al., 2005; Domagal-Goldman & Kubicki., 2008; Ottonello & Zuccolini., 2009; Rustad et al., 2010; Moynier et al., 2013; Fujii et al., 2014	Calculated $10^3Ln^{56}\alpha_{A-B}$	$10^3Ln^{56}\alpha_{FeII-FeIII}$	-3.09 ± 0.75‰
Complexation (Abiotic/experimental)			
Dideriksen et al., 2008	Abiotic FeIII-DFOB	$\Delta^{56}Fe_{FeIII-DFOB}$	-0.60 ± 0.15‰
Morgan et al., 2010	Abiotic FeIII-DFOB to FeIII-Ox	$\Delta^{56}Fe_{(FeIII-DFOB)-(FeIII-Ox)}$	0.20 ± 0.11‰
	Abiotic FeIII-DFOB to FeIII-EDTA	$\Delta^{56}Fe_{(FeIII-DFOB)-(FeIII-EDTA)}$	0.02 ± 0.11‰
Lotfi-Kalahroodi et al., 2019	Abiotic organic matter binding to FeIII at pH 6.5	$\Delta^{56}Fe_{TotFe-<0.2\mu m}$	-0.07 ± 0.08‰
		$\Delta^{56}Fe_{TotFe->0.2\mu m}$	0.05 ± 0.08‰
		$\Delta^{56}Fe_{TotFe-<30\ kDa}$	-0.35 ± 0.08‰
		$\Delta^{56}Fe_{TotFe->30\ kDa}$	0.00 ± 0.08‰
		$\Delta^{56}Fe_{TotFe-(0.2\ \mu m-30\ kDa)}$	-0.08 ± 0.08‰
Dissolution (Abiotic)			
Brantley et al., 2001a	*Bacillus mycoides* & *Streptomyces sps*.	$\Delta^{56}Fe_{solution-Silicates}$	0.48 ± 0.29‰
Brantley et al., 2001b; Brantley et al., 2004; Kiczka et al., 2010	Abiotic Silicates + ligands		-0.32 ± 0.13‰
Brantley et al.. 2004	*Bacillus mycoides* & *Streptomyces sps*.	$\Delta^{56}Fe_{solution-Goethite}$	-1.44 ± 0.17‰
Wiederhold et al., 2006; Jang et al., 2008	Abiotic Goethite + ligands		-1.32 ± 0.34‰
Wolfe et al.. 2016	Abiotic Pyrite + ligands	$\Delta^{56}Fe_{solution-Pyrite}$	-0.34 ± 0.61‰
Precipitation (Abiotic)			
Skulan et al., 2002; Beard et al., 2010	Abiotic experiment	$\Delta^{56}Fe_{III-Hematite-Kinetic}$	1.30 ± 0.12‰
		$\Delta^{56}Fe_{III-Hematite-Equilibrium}$	-0.15 ± 0.20‰
Fujii et al., 2014; Polyakov et al., 2007	Calculated $10^3Ln^{56}\alpha_{A-B}$	$10^3Ln^{56}\alpha_{FeIII-Hematite}$	0.29 ± 0.70‰
Wiesli et al., 2004	Abiotic experiment	$\Delta^{56}Fe_{II-Siderite-Kinetic}$	0.04 ± 0.10‰
		$\Delta^{56}Fe_{II-Siderite-Equilibrium}$	0.48 ± 0.22‰
Fujii et al., 2014; Blanchard et al., 2009	Calculated $10^3Ln^{56}\alpha_{A-B}$	$10^3Ln^{56}\alpha_{FeII-Siderite}$	0.89 ± 0.45‰

Butler et al., 2005; Guilbaud et al., 2010; Guilbaud et al., 2011a	Abiotic experiment	$\Delta^{56}Fe_{II\text{-}Mackinawite\text{-}Kinetic}$	0.85 ± 0.30‰
		$\Delta^{56}Fe_{II\text{-}Mackinawite\text{-}Equilibrium}$	-0.33 ± 0.16‰
Fujii et al., 2014; Polyakov & Soultanov., 2011	Calculated $10^3Ln^{56}\alpha_{A\text{-}B}$	$10^3Ln^{56}\alpha_{FeII\text{-}Mackinawite}$	3.17 ± 0.45‰
Mansor and Fantle et al., 2019	Abiotic experiment	$\Delta^{56}Fe_{II\text{-}Pyrite\text{-}Kinetic}$	0.75 ± 0.15‰
		$\Delta^{56}Fe_{II\text{-}Pyrite\text{-}Equilibrium}$	0.44 ± 0.15‰
Fujii et al., 2014; Polyakov & Soultanov., 2011	Calculated $10^3Ln^{56}\alpha_{A\text{-}B}$	$10^3Ln^{56}\alpha_{FeII\text{-}Pyrite}$	-5.74 ± 0.45‰
Bio-oxidation & Bio-mineralization			
Croal et al., 2004	*Thiodictyon strain F4*	$\Delta^{56}Fe_{FeII\text{-}FeIII\text{-}FeIIISolid}$	-2.09 ± 0.05‰
Kappler et al., 2010	*Acidovorax sp. BoFeN1*		-2.94 ± 0.05‰
Swanner et al., 2015	*Rhodovulum iodosum*		-1.99 ± 0.24‰
Swanner et al., 2017	*Synechococcus PCC7002*		-3.35 ± 0.19‰
Fujii et al., 2014; Polyakov and Mineev, 2000	Calculated $10^3Ln^{56}\alpha_{A\text{-}B}$	$\Delta^{56}Fe_{II\text{-}III\text{-}Goethite}$	-0.72 ± 0.45‰
		$\Delta^{56}Fe_{II\text{-}III\text{-}Lepidocrocite}$	-0.34 ± 0.45‰
Amor et al., 2016	*Magnetospirillum Magneticum strain AMB-1 (MDF)*	$\Delta^{56}Fe_{II\text{-}Magnetite}$	1.39 ± 0.19‰
		$\Delta^{56}Fe_{III\text{-}Magnetite}$	2.15 ± 0.18‰
		$\Delta^{56}Fe_{II\text{-}Lysate}$	-0.80 ± 0.08‰
		$\Delta^{56}Fe_{III\text{-}Lysate}$	-0.48 ± 0.17‰
	Magnetospirillum Magneticum strain AMB-1 (MIF)	$\Delta^{57}Fe_{II\text{-}Magnetite}$	-0.06 ± 0.08‰
		$\Delta^{57}Fe_{III\text{-}Magnetite}$	-0.24 ± 0.04‰
		$\Delta^{57}Fe_{II\text{-}Lysate}$	-0.02 ± 0.03‰
		$\Delta^{57}Fe_{III\text{-}Lysate}$	-0.04 ± 0.00‰
Fujii et al., 2014; Polyakov (personal communication)	Calculated $10^3Ln^{56}\alpha_{A\text{-}B}$	$10^3Ln^{56}\alpha_{FeII\text{-}Magnetite}$	-1.22 ± 0.45‰
		$10^3Ln^{56}\alpha_{FeIII\text{-}Magnetite}$	1.75 ± 0.70‰

743

744 Table 3. Theoretical calculations of ($10^3 Ln\beta^{56/54}$) for different redox of Fe complex to different organic and inorganic ligands in respect to bond

745 length (Å) when available.

	Bond length (Å)	$10^3 Ln\beta^{56/54}$ for FeIIcomplex		Bond length (Å)	$10^3 Ln\beta^{56/54}$ for FeIIIComplex
$[Fe_{II}(H_2O)_6]^{2+}$	2.16	5.4	$[Fe_{III}(H_2O)_6]^{3+}$	2.06	8.7
$=[(CH_3COO)Fe_{II}]^{+}$	n.a	2.42	$=[(CH_3COO)Fe_{III}]_2^{+}$	n.a	3.42
$[Fe_{II}(Ox)_3]^{4-}$	2.15	5.50	$[Fe_{III}(Ox)_3]^{3-}$	2.00	7.70
$[Fe_{II}(Cat)_3]^{4-}$	2.20	4.91	$[Fe_{III}(Cat)_3]^{3-}$	2.05	7.27
$Fe_{II}(cit)_2OH^{5-}$	n.a	5.25	$Fe_{III}(cit)_2OH^{4-}$	n.a	8.93
$Fe_{II}Cl_2(H_2O)_4$	2.25	4.64	$Fe_{III}Cl_2(H_2O)_4^{+}$	2.15	6.87
$Fe_{II2}(OH)_6^{2-}$	1.88	5.41	$Fe_{III}(OH)_3(H_2O)_3$	1.75	9.39
$Fe_{II}SO_4(H_2O)_5$	1.92	5.40	$Fe_{III}SO_4(H_2O)_5^{+}$	1.80	8.42
$Fe_{II}CO_3(H_2O)_4$	2.04	5.81	$Fe_{III}CO_3(H_2O)_4^{+}$	1.92	7.85
$Fe_{II}HPO_4(H_2O)_5$	1.98	5.88	$Fe_{III}HPO_4(H_2O)_5^{+}$	1.84	9.12
Fe_{II}-HS	2.32	3.96			
(1) redox reactions of Fe within the same phosphate complex ($Fe_{II}HPO_4(H_2O)_5$ & $Fe_{III}HPO_4(H_2O)_5^{+}$), $\Delta^{56}Fe_{A-B}$(‰) is -3.24‰					
(2) the exchange between different inorganic ligands but the same Fe redox ($Fe_{III}HPO_4(H_2O)_5^{+}$ & $Fe_{III}CO_3(H_2O)_4^{+}$), $\Delta^{56}Fe_{A-B}$(‰) is 1.27‰					
(3) the exchange between inorganic and organic ligands but the same Fe redox ($Fe_{III}(cit)_2OH_4^{-}$ & $Fe_{III}Cl_2(H_2O)_4^{+}$), $\Delta^{56}Fe_{A-B}$(‰) is 2.06‰					

746 (References: Fujii et al., 2014; Ottonello and Zuccolini, 2008; Moynier, et al., 2013)

747 Table 4. Comparison of the equilibrium iron isotope fractionation obtained in experimental studies ($\Delta^{56}Fe_{A-B}$) to those obtained in spectroscopy

748 studies and theoretical calculations ($10^3Ln\beta^{56/54}$) for dissimilatory iron reduction.

Dissimilatory iron reduction					
References	**Scope of studies**	**Fe Pairs**	**$\Delta^{56}Fe_{IIaq-Bulk}$ (‰)**	**$\Delta^{56}Fe_{IIaq-FeIIsorbed}$ (‰)**	**$\Delta^{56}Fe_{IIaq-FeIIreac}$ (‰)**
Crosby et al., 2005 & 2007; Icopini et al., 2004	*Shewanella putrefaciens*	**$\Delta^{56}Fe_{FeIIaq-Goethite}$**	-0.89 ± 0.33‰	-0.86 ± 0.18‰	-2.62 ± 0.64‰
Beard et al., 2010; Frierdich et al., 2014; Reddy et al., 2015	Abiotic-micro-goethite	**$\Delta^{56}Fe_{FeIIaq-Micro-Goethite}$**	-1.05 ± 0.08‰	-1.24 ± 0.14‰	-1.68 ± 0.08‰
	Abiotic-nano-goethite	**$\Delta^{56}Fe_{FeIIaq-Nano-Goethite}$**	-1.22 ± 0.08‰	-1.24 ± 0.14‰	-2.10 ± 0.48‰
Fujii et al., 2014; Polyakov and Mineev, 2000	Calculated $10^3Ln^{56}\alpha_{A-B}$	**$10^3Ln^{56}\alpha_{FeII-Goethite}$**	-0.72 ± 0.45‰	-	-
Crosby et al., 2005; 2007 & Wu et al., 2009	*Shewanella putrefaciens, Geobacter sulfurreducens*	**$\Delta^{56}Fe_{FeIIaq-bulk-Hematite}$**	-1.56 ± 0.28‰	-0.30 ± 0.15‰	-2.95 ± 0.19‰
Wu et al., 2009	Abiotic experiment without Si, pH7		-	-0.49 ± 0.09‰	-2.64 ± 0.19‰
	Abiotic experiment with Si, pH7		-	-0.20 ± 0.13‰	-1.90 ± 0.47‰
	Abiotic experiment without Si, pH 8.7		-	-0.36 ± 0.13‰	-1.76 ± 0.21‰
	Abiotic FeIIaq and Fe-Si gel, pH 8.7		-	-0.51 ± 0.18‰	-2.66 ± 0.18‰
Wu et al., 2010; Frierdich et al., 2019; Skulan et al., 2002; Welch et al., 2003	Abiotic-Coarse-hematite ($7\ m^2g^{-1}$)		-3.10 ± 0.36‰	-0.83 ± 1.08‰	-
	Abiotic-Fine-hematite ($60\ m^2g^{-1}$)		-2.77 ± 0.37‰	-0.74 ± 0.45‰	-
Fujii et al., 2014; Polyakov et al., 2007	Calculated $10^3Ln^{56}\alpha_{A-B}$	**$10^3Ln^{56}\alpha_{FeII-Hematite}$**	-2.68 ± 0.45‰	-	-
Beard et al., 1999 & 2003	*Shewanella alga (Strain BrY and Strain BCMB)*	**$\Delta^{56}Fe_{FeIIaq-Ferrihydrite}$**	-1.30 ± 0.22‰	-	-
Wu et al., 2011	Abiotic pure HFO		-3.20 ± 0.10‰	-	-
	Abiotic HFO + Si		-3.17 ± 0.08‰	-	-
	Abiotic Si+HFO		-2.58 ± 0.14‰	-	-

Chanda et al., 2020	Abiotic C+HFO		-2.36 ± 0.26‰	-	-
n.a	Calculated $10^3Ln^{56}\alpha_{A-B}$	$\mathbf{10^3Ln^{56}\alpha_{FeII\text{-}Ferrihydrite}}$	n.a	-	-
Johnson et al., 2005	*Geobacter sulfurreducens*	$\mathbf{\Delta^{56}Fe_{II\text{-}Siderite}}$	0.00 ± 0.22‰	-	-
	Geobacter sulfurreducens + Ca-Sid		1.00 ± 0.22‰	-	-
Wiesli et al., 2004	Abiotic experiment		0.48 ± 0.22‰	-	-
Fujii et al., 2014; Blanchard et al., 2009	Calculated $10^3Ln^{56}\alpha_{A-B}$	$\mathbf{10^3Ln^{56}\alpha_{FeII\text{-}Siderite}}$	0.89 ± 0.45‰	-	-
Johnson et al., 2005	*Geobacter sulfurreducens*	$\mathbf{\Delta^{56}Fe_{FeII(aq)\text{-}bulk\text{-}Magnetite}}$	-1.34 ± 0.22‰	-	-
Frierdich et al., 2014b	Abiotic experiment		-1.56 ± 0.22‰	-	-
	Abiotic Magnetite from HFO		-1.61 ± 0.22‰	-	-
Fujii et al., 2014; Polyakov (personal communication)	Calculated $10^3Ln^{56}\alpha_{A-B}$	$\mathbf{10^3Ln^{56}\alpha_{FeII\text{-}Magnetite}}$	-1.22 ± 0.45‰	-	-

749

5. Outlook

A very limited number of studies addressed iron isotope fractionation during microbial uptake. Microbial ferrous oxidation and adsorption are areas where our understanding remains rather poor given the large discrepancies observed; it could be due to microbial diversity, cell structure, metabolic pathways, the mechanisms involved, as well as to experimental and analytical artifacts arisen from sample preparation. In addition, the role of microbial secreted ligands such as siderophores and how it contributes to the overall iron isotope fractionation in aquatic environment is still unknown. Several abiotic experimental studies have focused on using three-isotope-techniques to mathematically achieve the equilibrium isotope fractionation from the kinetic driven experiment, as a way to decipher kinetic and equilibrium isotope effects. However, it is still unknown how the presence of microorganisms could influence and shift such isotope effects.

Our review suggests that significant fractionation of iron isotopes occurs in low-temperature environments, where the extent of fractionation is greatly governed by several biogeochemical processes such as redox reaction, alteration, complexation, adsorption, oxidation and reduction, with or without the influence of microorganisms. Many challenges remain to untangle the isotope signature when all of these processes are taking place at the same time; to decipher the biotic influence from abiotic one, to adequately differentiate kinetic fractionation from equilibrium fractionation, to understand the microbial fractionation at a cellular level, and how the microbial diversity, cell structure and different metabolic pathway contributes to the overall fractionation. A great deal of work is also still required to disentangle the abiotic iron mineral precipitation from biogenic mineral formation. Therefore the mineral transformation pathway coupled to the iron isotope fractionation pathway could be a way to a better comprehension of the iron mineral cycle in nature. This review thus presents several opportunities for future work on iron isotope fractionation in low-temperature biogeochemical environment.

Acknowledgement

This work is supported by Université de Pau et des Pays de l'Adour (UPPA) in the framework of Energy Environment Solutions (E2S) for the project “Metals in Environmental Systems Microbiology (MeSMic)”. Special thanks to Mr James Ash (Nu Instruments Ltd, UK) for his kind assistance in English proofing of the manuscript.

780 **References**

781 1. Amor, M., Busigny, V., Louvat, P., Gélabert, A., Cartigny, P., Durand-Dubief, M., Ona-
782 Nguema, G., Alphandéry, E., Chebbi, I., Guyot, F., 2016. Mass-dependent and –
783 independent signature of Fe isotopes in magnetotactic bacteria. Science, 352, 705–708.
784 https://doi.org/10.1016/j.gca.2004.06.012.
785 2. Anbar, A.D., Jarzecki, A.A., Spiro, T.G., 2005. Theoretical investigation of iron isotope
786 fractionation between $Fe(H_2O)_6^{3+}$ and $Fe(H_2O)_6^{2+}$: Implications for iron stable isotope
787 geochemistry. Geochim. Cosmochim. Acta. 69, 825–837.
788 https://doi.org/10.126/science.aad7632.
789 3. Beard, B.L., Johnson, C.M., Cox, L., Sun, H., Nealson, K.H., Aguilar, C., 1999. Iron
790 isotope biosignatures. Science. 285, 1889–1892.
791 https://doi.org/10.1126/science.285.5435.1889.
792 4. Beard, B.L., Johnson, C.M., Skulan, J.L., Nealson, K.H., Cox, L., Sun, H., 2003.
793 Application of Fe isotopes to tracing the geochemical and biological cycling of Fe.
794 Chem. Geol. 195, 87–117. https://doi.org/10.1016/S0009-2541(02)00390-X.
795 5. Beard, B.L., Johnson, C.M., 2004. Inter-mineral Fe isotope variations in mantle-derived
796 rocks and implications for the Fe geochemical cycle. Geochimica et Cosmochimica
797 Acta. 68, 4727-4743, 2004. https://doi:10.1016/j.gca.2004.04.023.
798 6. Beard, B.L., Handler, R.M., Scherer, M.M., Wu, L., Czaja, A.D., Heimann, A., Johnson,
799 C.M., 2010. Iron isotope fractionation between aqueous ferrous iron and goethite. Earth
800 Planet. Sci. Lett. 295, 241–250. https://doi.org/10.1016/j.epsl.2010.04.006.
801 7. Blanchard, M., Poitrasson, F., Méheut, M., Lazzeri, M., Mauri, F., Balan, E., 2009. Iron
802 isotope fractionation between pyrite (FeS_2), hematite (Fe_2O_3) and siderite ($FeCO_3$): A
803 first-principles density functional theory study. Geochim. Cosmochim. Acta. 73, 6565-
804 6578. https://doi.org/10.1016/j.gca.2009.07.034.

8. Brantley S. L., Liermann L. J., Bau M., and Wu S. (2001a) Uptake of trace metals and rare earth elements from hornblende by a soil bacterium. Geomicrobiol. J. 18, 37–61.
9. Brantley S. L., Liermann L. J., and Bullen T. D. (2001b) Fractionation of. Fe isotopes by soil microbes and organic acids. Geology 29, 535–538. https://doi.org/10.1130/0091-7613(2001)029<0535:FOFIBS>2.0.CO;2.
10. Brantley, S.L., Liermann, L.J., Guynn, R.L., Anbar, A., Icopini, G.A., Barling, J., 2004. Fe isotopic fractionation during mineral dissolution with and without bacteria. Geochim. Cosmochim. Acta. 68, 3189–3204. https://doi.org/10.1016/j.gca.2004.01.023.
11. Butler, I.B., Archer, C., Vance, D., Oldroyd, A., Rickard, D., 2005. Fe isotope fractionation on FeS formation in ambient aqueous solution. Earth Planet. Sci. Lett. 236, 430–442. https://doi.org/10.1016/j.epsl.2005.05.022.
12. Chanda, P., Zhou, Z., Latta, D.E., Scherer, M.M., Beard, B.L., Johnson, C.M., 2020. Effect of organic C on stable Fe isotope fractionation and isotope exchange kinetics between aqueous Fe(II) and ferrihydrite at neutral pH. Chem. Geol. 531, 119344. https://doi.org/10.1016/j.chemgeo.2019.119344.
13. Crichton, R.R. (2001). Inorganic Biochemistry of Iron Metabolism: From Molecular Mechanisms to Clinical Consequences. 2nd edn. John Wiley & Sons Ltd, Chichester, 326 pp.
14. Croal, L.R., Johnson, C.M., Beard, B.L., Newman, D.K., 2004. Iron isotope fractionation by Fe(II)-oxidizing photoautotrophic bacteria. Geochim. Cosmochim. Acta. 68, 1227–1242. https://doi.org/10.1016/j.gca.2003.09.011.
15. Crosby, H.A., Johnson, C.M., Roden, E.E., Beard, B.L., 2005. Coupled Fe(II)-Fe(III) electron and atom exchange as a mechanism for Fe isotope fractionation during dissimilatory iron oxide reduction. Environ. Sci. Technol. 39, 6698–6704. https://doi.org/10.1021/es0505346.

16. Crosby, H.A., Roden, E.E., Johnson, C.M., Beard, B.L., 2007. The mechanisms of iron isotope fractionation produced during dissimilatory Fe(III) reduction by Shewanella putrefaciens and Geobacter sulfurreducens. Geobiology. 5, 169–189. https://doi.org/10.1111/j.1472-4669.2007.00103.x.

17. Dauphas, N., Rouxel, O., 2006. Mass spectrometry and natural variations of iron isotopes. Mass Spectrom. Rev. 25, 515–550. https://doi.org/10.1002/mas.20078.

18. Dauphas, N., Schauble, E., 2016. Mass fractionation laws, mass-independent effects, isotopic anomalies. Ann. Rev. Earth Planet Sci. 44, 709–783. https://doi.org/10.1146/annurev-earth-060115-012157.

19. Dauphas, N., John, S., Rouxel, O., 2017. Iron isotope systematics. Rev. Mineral. Geochem. 82, 415–510. https://doi.org/10.2138/rmg.2017.82.11.

20. Dideriksen, K., Baker, J.A., Stipp, S.L.S., 2008. Equilibrium Fe isotope fractionation between inorganic aqueous Fe(III) and the siderophore complex, Fe(III)-desferrioxamine B. Earth Planet. Sci. Lett. 269, 280–290. https://doi.org/10.1016/j.epsl.2008.02.022.

21. Domagal-Goldman, S.D., Kubicki, J.D., 2008. Density functional theory predictions of equilibrium isotope fractionation of iron due to redox changes and organic complexation. Geochim. Cosmochim. Acta. 72, 5201-5216. https://doi.org/10.1016/j.gca.2008.05.066.

22. Frierdich, A.J., Beard, B.L., Reddy, T.R., Scherer, M.M., Johnson, C.M., 2014a. Iron isotope fractionation between aqueous Fe(II) and goethite revisited: New insights based on a multi-direction approach to equilibrium and isotopic exchange rate modification. Geochim. Cosmochim. Acta. 139, 383-398, https://doi.org/10.1016/j.gca.2014.05.001.

23. Frierdich, A.J., Beard, B.L., Scherer, M.M., Johnson, C.M., 2014b. Determination of the Fe(II)aq–magnetite equilibrium iron isotope fractionation factor using the three-

isotope method and a multi-direction approach to equilibrium. Earth Planet. Sci. Lett. 391, 77-86, https://doi.org/10.1016/j.epsl.2014.01.032.

24. Frierdich, A.J., Helgeson, M., Liu, C., Wang, C., Rosso, K. M., Scherer, M.M., 2015. Iron Atom Exchange between Hematite and Aqueous Fe(II). Environ. Sci. Technol. 49, 8479−8486. https://doi.org/10.1021/acs.est.5b01276.
25. Frierdich, A.J., Nebel, O., Beard, B.L., Johnson, C.M., 2019. Iron isotope exchange and fractionation between hematite (α-Fe_2O_3) and aqueous Fe(II): A combined three-isotope and reversal-approach to equilibrium study. Geochim. Cosmochim. Acta. 245, 207–221. https://doi.org/10.1016/j.gca.2018.10.033.
26. Fujii, T., Moynier, F., Blichert-Toft, J., Albarède, F., 2014. Density functional theory estimation of isotope fractionation of Fe, Ni, Cu, and Zn among species relevant to geochemical and biological environments, Geochim. Cosmochim. Acta. 140, 553-576. https://doi.org/10.1016/j.gca.2014.05.051.
27. Gorski, C.A., Handler, R.M., Beard, B.L., Pasakarnis, T., Johnson, C.M., Scherer, M.M., 2012. Fe atom exchange between aqueous Fe^{2+} and magnetite. Environ. Sci. Technol. 46, 12399-12407. https://doi.org/10.1021/es204649a.
28. Guilbaud, R., Butler, I.B., Ellam, R.M., Rickard, D., 2010. Fe isotope exchange between Fe(II)aq and nanoparticulate mackinawite (FeSm) during nanoparticle growth. Earth Planet. Sci. Lett. 300, 174–183. https://doi.org/10.1016/j.epsl.2010.10.004.
29. Guilbaud, R., Butler, I.B., Ellam, R.M., 2011a. Abiotic pyrite formation produces a large Fe isotope fractionation. Science. 332, 1548–1551. https://doi.org/10.1126/science.1202924.
30. Handler, R.M., Beard, B.L., Johnson, C.M., Scherer, M.M., 2009. Atom exchange between aqueous Fe (II) and goethite: An Fe isotope tracer study. Environ. Sci. Technol. 43, 1102-1107. https://doi.org/10.1021/es802402m.

880 31. Hill, P.S., Schauble, E.A., Shahar, A., Tonui, E., Young, E.D., 2009. Experimental
881 studies of equilibrium iron isotope fractionation in ferric aquo–chloro complexes.
882 Geochim. Cosmochim. Acta. 73, 2366–2381.
883 https://doi.org/10.1016/j.gca.2009.01.016.
884 32. Icopini, G.A., Anbar, A.D., Ruebush, S.S., Tien, M., Brantley, S.L., 2004. Iron isotope
885 fractionation during microbial reduction of iron: The importance of adsorption.
886 Geology. 32, 205–208. https://doi.org/10.1130/G20184.1.
887 33. Jang, J.-H., Mathur, R., Liermann, L.J., Ruebush, S., Brantley, S.L., 2008. An iron
888 isotope signature related to electron transfer between aqueous ferrous iron and goethite.
889 Chem. Geol. 250, 40–48. https://doi.org/10.1016/j.chemgeo.2008.02.002.
890 34. Jimenez-Lopez, C., Romanek, C. S., and Bazylinski, D. A. (2010). Magnetite as a
891 prokaryotic biomarker: A review. J. Geophys. Res. 115, G00G03.
892 doi:10.1029/2009JG001152.
893 35. Johnson, C.M., Skulan, J.L., Beard, B.L., Sun, H., Nealson, K.H., Braterman, P.S.,
894 2002. Isotopic fractionation between Fe(III) and Fe(II) in aqueous solutions. Earth
895 Planet. Sci. Lett. 195, 141–153. https://doi.org/10.1016/S0012-821X(01)00581-7.
896 36. Johnson, C.M., Roden, E.E., Welch, S.A., Beard, B.L., 2005. Experimental constraints
897 on Fe isotope fractionation during magnetite and Fe carbonate formation coupled to
898 dissimilatory hydrous ferric oxide reduction. Geochim. Cosmochim. Acta. 69, 963–993.
899 https://doi.org/10.1016/j.gca.2004.06.043.
900 37. Johnson, C.M., Beard, B., Weyer, S., 2020. Iron Geochemistry: An Isotopic Perspective.
901 Springer International Publishing. https://10.1007/978-3-030-33828-2.
902 38. Kappler, A., Johnson, C.M., Crosby, H.A., Beard, B.L., Newman, D.K., 2010. Evidence
903 for equilibrium iron isotope fractionation by nitrate-reducing iron(II)-oxidizing bacteria.

904 Geochim. Cosmochim. Acta. 74, 2826–2842.
905 https://doi.org/10.1016/j.gca.2010.02.017.
906 39. Kiczka, M., Wiederhold, J.G., Frommer, J., Kraemer, S.M., Bourdon, B., Kretzschmar,
907 R., 2010a. Iron isotope fractionation during proton- and ligand-promoted dissolution of
908 primary phyllosilicates. Geochim. Cosmochim. Acta. 74, 3112–3128.
909 https://doi.org/10.1016/j.gca.2010.02.018.
910 40. Mansor, M., Fantle, M.S., 2019. A novel framework for interpreting pyrite-based Fe
911 isotope records of the past. Geochim. Cosmochim. Acta. 253, 39-62.
912 https://doi.org/10.1016/j.gca.2019.03.017.
913 41. Miot, J., Benzerara, K., Obst, M., Kappler, A., Hegler, F., Schadler, S., Bouchez, C.,
914 Guyot, F., Morin, G., 2009. Extracellular Iron Biomineralization by Photoautotrophic
915 Iron-Oxidizing Bacteria. Applied and environmental microbiology. 75. 5586-91.
916 https://doi.org/10.1128/AEM.00490-09.
917 42. Mikutta, C., Wiederhold, J.G., Cirpka, O.A., Hofstetter, T.B., Bourdon, B., Von Gunten,
918 U., 2009. Iron isotope fractionation and atom exchange during sorption of ferrous iron
919 to mineral surfaces. Geochim. Cosmochim. Acta. 73, 1795–1812.
920 https://doi.org/10.1016/j.gca.2009.01.014.
921 43. Morgan J. L. L., Wasylenki L. E., Nuester J. and Anbar A. D., 2010. Fe isotope
922 fractionation during equilibration of Fe organic complexes. Environ. Sci. Technol. 44,
923 6095–6101. https://doi.org/10.1021/es100906z.
924 44. Moynier, F., Fujii, T., Wang, K., Foriel, J., 2013. Ab initio calculations of the Fe (II)
925 and Fe (III) isotopic effects in citrates, nicotianamine, and phytosiderophore, and new
926 Fe isotopic measurements in higher plants. Compt. Rend. Geosci. 345, 230-240.
927 https://doi.org/10.1016/j.crte.2013.05.003.

928 45. Mulholland, D.S., Poitrasson, F., Shirokova, L.S., González, A.G., Pokrovsky, O.S.,
929 Boaventura, G.R., Vieira, L.C., 2015b. Iron isotope fractionation during Fe(II) and Fe(III)
930 adsorption on cyanobacteria. Chem. Geol. 400, 24–33.
931 https://doi.org/10.1016/j.chemgeo.2015.01.017.
932 46. Ottonello, G., Zuccolini, M.V., 2008. The iron-isotope fractionation dictated by the
933 carboxylic functional: An ab-initio investigation. Geochim. Cosmochim. Acta. 72,
934 5920–5934. https://doi.org/10.1016/j.gca.2008.09.027.
935 47. Ottonello, G., Zuccolini M.V., 2009. Ab-initio structure, energy and stable Fe isotope
936 equilibrium fractionation of some geochemically relevant H–O–Fe complexes.
937 Geochim. Cosmochim. Acta. 73, 6447–6469.
938 https://doi.org/10.1016/j.gca.2009.06.034.
939 48. Peiffer, S., Behrends, T., Hellige, K., Larese-Casanova, P., Wan, M. and Pollok, K.
940 (2015) Pyrite formation and mineral transformation pathways upon sulfidation of ferric
941 hydroxides depend on mineral type and sulphide concentration. Chem. Geo. 400, 44-
942 55. http://dx.doi.org/10.1016%2Fj.chemgeo.2015.01.023.
943 49. Polyakov, V.B., Mineev, S.D., 2000. The use of Mössbauer spectroscopy in stable
944 isotope geochemistry. Geochim. Cosmochim. Acta. 64, 849–865.
945 https://doi.org/10.1016/S0016-7037(99)00329-4.
946 50. Polyakov, V.B., Clayton, R.N., Horita, J., Mineev, S.D., 2007. Equilibrium iron isotope
947 fractionation factors of minerals: Reevaluation from the data of nuclear inelastic
948 resonant X-ray scattering and Mössbauer spectroscopy. Geochim. Cosmochim. Acta.
949 71, 3833-3846. https://doi.org/10.1016/j.gca.2007.05.019.
950 51. Polyakov, V.B., Soultanov, D.M., 2011. New data on equilibrium iron isotope
951 fractionation among sulfides: Constraints on mechanisms of sulfide formation in
952 hydrothermal and igneous systems. Geochim. Cosmochim. Acta. 75, 1957-1974.
953 https://doi.org/10.1016/j.gca.2011.01.019.

52. Polyakov, V.B, Osadchii, E.G., Chareev, D.A., Chumakov, A.I., Sergeev, I.A., 2013. Fe β-factors for sulfides from NRIXS synchrotron experiments. Mineralogical Magazine, 77(5) 1985. https://doi.org/10.1180/minmag.2013.077.5.16.

53. Reddy, T.R., Frierdich, A.J., Beard, B.L., Johnson, C.M., 2015. The effect of pH on stable iron isotope exchange and fractionation between aqueous Fe(II) and goethite. Chem. Geol. 397, 118–127. https://doi.org/10.1016/j.chemgeo.2015.01.018.

54. Rickard, R., Butler, I.B., Oldroyd, A., 2001. A novel iron sulphide mineral switch and its implications for Earth and planetary science. Earth Planet. Sci. Lett. 189, 85-91. https://doi.org/10.1016/S0012-821X(01)00352-1.

55. Roe J. E., Anbar A. D. and Barling J., 2003. Nonbiological fractionation of Fe isotopes: Evidence of an equilibrium isotope effect. Chem. Geol. 195, 69–85. https://doi.org/10.1016/S0009-2541(02)00389-3.

56. Rustad, J.R., Casey, W.H., Yin, Q.Z., Bylaska, E.J., Felmy, A.R., Bogatko, S.A., Jackson, V.E., Dixon, D.A., 2010. Isotopic fractionation of $Mg^{2+}_{(aq)}$, $Ca^{2+}_{(aq)}$, and $Fe^{2+}_{(aq)}$ with carbonate minerals. Geochim. Cosmochim. 74, 6301–6323. https://doi.org/10.1016/j.gca.2010.08.018.

57. Skulan, J.L., Beard, B.L., Johnson, C.M., 2002. Kinetic and equilibrium Fe isotope fractionation between aqueous Fe(III) and hematite. Geochim. Cosmochim. Acta. 2002 (66), 2995–3015. https://doi.org/10.1016/S0016-7037(02)00902-X.

58. Sun, R., Wang, B., 2018. Iron isotope fractionation during uptake of ferrous ion by phytoplankton. Chem. Geol. 481, 65–73. https://doi.org/10.1016/j.chemgeo.2018.01.031.

59. Swanner, E.D., Wu, W., Schoenberg, R., Byrne, J., Michel, F.M., Pan, Y., Kappler, A., 2015. Fractionation of Fe isotopes during Fe(II) oxidation by a marine photoferrotroph

978 is controlled by the formation of organic Fe-complexes and colloidal Fe fractions.
979 Geochim. Cosmochim. Acta. 165, 44–61. https://doi.org/10.1016/j.gca.2015.05.024.
980 60. Swanner, E.D., Bayer, T., Wu, W., Hao, L., Obst, M., Sundman, A., Byrne, J.M.,
981 Michel, F.M., Kleinhanns, I.C., Kappler, A., Schoenberg, R., 2017. Iron isotope
982 fractionation during Fe(II) oxidation mediated by the oxygen-producing marine
983 cyanobacterium Synechococcus PCC 7002. Environ. Sci. Technol. 51, 4897–4906.
984 https://doi.org/10.1021/acs.est.6b05833.
985 61. USEPA 1986. Quality criteria for water. US Department of Commerce, National
986 Technical Information Service, US Environmental Protection Agency, Springfield,
987 Virginia. PB87-226759, EPA 440/5 86-001.
988 62. Wan, M., Schröder, C., Peiffer, S., 2017. Fe(III):S(-II) Concentration Ratio Controls the
989 Pathway and the Kinetics of Pyrite Formation during Sulfidation of Ferric Hydroxides,
990 Geochim. Cosmochim. 217, 334-348. DOI: 10.1016/j.gca.2017.08.036.
991 63. Wang, X., Zhu, M., Koopal, L.K., Li, W., Xu, W., Liu, F., Zhang, J., Liu, Q., Feng, X.,
992 Sparks, D.L., 2016. Effects of crystallite size on the structure and magnetism of
993 ferrihydrite. Environ. Sci. Nano 3, 190–202. https://doi.org/10.1039/C5EN00191A.
994 64. Wasylenki, L.E., Anbar, A.D., Liermann, L.J., Mathur, R., Gordona, G.W., Brantley,
995 S.L., 2007. Isotope fractionation during microbial metal uptake measured by MC-ICP-
996 MS. J. Anal. At. Spectrom. 22, 905–910. https://doi.org/10.1039/b705476a.
997 65. Wehrli, B. (1990). Redox reactions of metal Ions at mineral surfaces. In W. Stumm
998 (Ed.), Aquatic Chemical Kinetics (pp. 311-336). Wiley.
999 66. Welch, S.A., Beard, B.L., Johnson, C.M., Braterman, P.S., 2003. Kinetic and
1000 equilibrium Fe isotope fractionation between aqueous Fe(II) and Fe(III). Geochim.
1001 Cosmochim. Acta. 67, 4231–4250. https://doi.org/10.1016/S0016-7037(03)00266-7.

1002 67. Wiederhold, J.G., Kraemer, S.M., Teutsch, N., Borer, P.M., Halliday, A.N.,
1003 Kretzschmar, R., 2006. Iron isotope fractionation during proton-promoted, ligand-
1004 controlled, and reductive dissolution of goethite. Environ. Sci. Technol. 40, 3787–3793.
1005 https://doi.org/10.1021/es052228y.
1006 68. Wiesli, R.A., Beard, B.L., Johnson, C.M., 2004. Experimental determination of Fe
1007 isotope fractionation between aqueous Fe(II), siderite and "green rust" in abiotic
1008 systems. Chem. Geol. 211, 343–362. https://doi.org/10.1016/j.chemgeo.2004.07.002.
1009 69. Wolfe, A.L., Stewart, B.W., Capo, R.C., Liu, R., Dzombak, D.A., Gordon, G.W., Anbar,
1010 A.D., 2016. Iron isotope investigation of hydrothermal and sedimentary pyrite and their
1011 aqueous dissolution products. Chem. Geol. 427, 73–82.
1012 https://doi.org/10.1016/j.chemgeo.2016.02.015.
1013 70. Wu, L., Beard, B.L., Roden, E.E., Johnson, C.M., 2009. Influence of pH and dissolved
1014 Si on Fe isotope fractionation during dissimilatory microbial reduction of hematite.
1015 Geochim. Cosmochim. Acta. 73, 5584–5599.
1016 https://doi.org/10.1016/j.gca.2009.06.026.
1017 71. Wu, L., Beard, B.L., Roden, E.E., Johnson, C.M., 2011. Stable iron isotope fractionation
1018 between aqueous Fe(II) and hydrous ferric oxide. Environ. Sci. Technol. 45, 1847–
1019 1852. https://doi.org/10.1021/es103171x.
1020 72. Wu, B., Amelung, W., Xing, Y., Bol, R., Berns, A.E., 2019. Iron cycling and isotope
1021 fractionation in terrestrial ecosystems. Earth. Sci. Rev. 190, 323-352.
1022 https://doi.org/10.1016/j.earscirev.2018.12.012.
1023 73. Zhou, Z., Latta, D.E., Noor, N., Thompson, A., Borch, T., Scherer, M.M., 2018. Fe(II)-
1024 catalyzed transformation of organic matter-ferrihydrite coprecipitates: a closer look
1025 using Fe isotopes. Environ. Sci. Technol. 52, 11142–11150.
1026 https://doi.org/10.1021/acs.est.8b03407.

Highlights

- Extent of Fe isotope fractionation depends on different geochemical processes
- Source signature of the original Fe minerals can be the primary control
- Limitations due to overlapping signatures between abiotic and biotic influences
- Reconciling the discrepancies observed between predicted and experimental values
- Microbial driven fractionation at inter/extracellular levels for future direction

Declaration of interests

☒ The authors declare that they have no known competing financial interests or personal relationships that could have appeared to influence the work reported in this paper.

☐The authors declare the following financial interests/personal relationships which may be considered as potential competing interests: